MEASURE OF SURFACE TEMPERATURES IN CITIES: FROM SATELLITE TO GROUND-BASED REMOTE SENSING

TECHNICAL REPORT
Elena GARCIA NEVADO and Benoit BECKERS
Urban Physics Joint Laboratory,
E2S UPPA, Université de Pau et des pays de l'Adour, 2021

Index

Term	Abbreviation
Urban Heat Island	UHI
Surface Urban Heat Island	SUHI
Land surface temperature	LST
Land surface emissivity	LSE
Top of the atmosphere	TOA
Normalized Difference Vegetation Index	NDVI

Infrared nomenclature	Abbreviation	Wavelength	Temperature	
Near-infrared	NIR	0.75–1.4 µm	3864– 2070 K	3591–1797 °C
Short-wavelength infrared	SWIR	1.4–3 µm	2070–966 K	1797–693 °C
Mid-wavelength infrared	MWIR	3–8 µm	966–362 K	693–89 °C
Long-wavelength or thermal infrared	LWIR / TIR	8–15 µm	362–193 K	89 – (−80 °C)

1. Introduction and aim of the document

Surface temperatures are of prime importance to the study of urban climate (J. A. Voogt & Oke, 2003). The retrieval of such information is a challenging task since the surface temperature of the urban skin varies considerably - both in time and space- due to differences in the energy balance of the individual facets.

Thermal remote sensing (RS) is a valuable information source in this regard because it provides a non-contact method to obtain spatialized thermal information of a surface at specific times, with various spatial and temporal resolutions. In urban settings, the RS quantification of surface temperature is tricky due to two factors. First, deriving actual temperatures from at-sensor radiances requires several corrections, which depend on hard-to-obtain data about urban surfaces (geometry, material properties, and boundary conditions). Second, as remote sensing is a view-dependent technique, capturing information about the convoluted urban surface can be tricky. **This report aims to overview how satellite, airborne, and ground-based RS observations address these issues.**

Satellite thermal infrared imagery (TIR), initially developed for military purposes, has a wide range of civil applications within different fields today (e.g., (Jose A. Sobrino et al., 2016) cited more than 30). Since the early '70s (Rao, 1972), this technique has been routinely used to retrieve land surface temperature for investigating **multiple aspects of urban climates**. Three central topics have been the study of urban surface energy balances, the correlation between surface characteristics and thermal patterns, and the urban heat island phenomenon (J. A. Voogt & Oke, 2003). *Section 2* outlines the main findings and research gaps in the latter field, one of the most active areas in climate research.

Over the last 50 years, satellite TIR remote sensing has decisively contributed to the understanding of climate dynamics at multiple scales. The findings of this discipline have had, though, **a limited impact on the construction of real cities** (Mills et al., 2010). One reason is that satellite thermography is **still too coarse** – both in time and space - to provide practical guidance for architectural interventions (*Section 3)*. Another reason is that satellite datasets are essentially **two-dimensional** while cities are three-dimensional by nature. Since the '90s (J. a. Voogt & Oke, 1997), climate researchers have implemented alternative RS approaches (airplane, drone, vehicle, platform, handheld cameras) to provide closer observations of the city from different view angles, to collect thermal data of the entire urban skin (*Section 4*).

Research using satellite TIR data has also been very prolific from the methodologic point of view. A significant number of approaches have been developed to **retrieve surface temperatures from satellite data** using various methods to correct the emissivity and atmospheric effects (Z. L. Li, Tang, et al., 2013). *Section 5* provides an **overview of these methods** and an example of how airborne urban studies inherited some of this knowledge. For several reasons, satellite algorithms are **not directly applicable** to ground-based thermography (*Section 6*). Yet, their approaches provide some **worth-exploring paths** to face the challenges of ground-based observations, key tools for the comprehension of urban microclimates (*Section 7*).

2. Satellite remote sensing for SUHI observations

Traditionally, the *Urban Heat Island* (UHI) refers to the differences in air temperature between urban and rural areas using pairs of *in situ* climatology data. The term *Surface Urban Heat Island* (SUHI) is used to distinguish UHIs measured using surface temperatures. SUHI has been widely used as a surrogate index to study the heat island effect indirectly.

Though first satellite-based observations of the SUHI phenomenon date back to the early seventies in US (Rao, 1972), this research field was not highly active until 2005. From then on, publications started to grow exponentially for three reasons (Zhou et al., 2019). First, a growing interest in urban climates due to rapid urbanization; second, the technical advances concerning remote sensing and computing power; third, the increase in freely available data. The use of satellite TIR imagery for UHI studies has multiple advantages, but this technique also presents significant limitations, regarding mainly the coverage of datasets and methodological constraints (Table 1).

Advantages	Limitations
Continuous spatial coverage compared to onsite data.	Data acquisition times of sun-synchronous satellites usually do not coincide with the time of day where the SUHI is at a minimum or maximum.
Provides data where no systematic onsite measurements are available and augments where they are.	The most widely used satellite for SUHI detection (i.e., Landsat) only has daytime data.
Simultaneous observations of LST, surface emissivity, and land cover from various satellites (e.g., Landsat/TM, ETM+, OLI & TIRS, MODIS, VIIRS, AVHRR).	Optical sensors cannot penetrate clouds or vegetative cover, which can lead to data gaps or a decrease in data utility.
Global, consistent, data coverage from many satellites.	The accuracy of land surface temperature (LST) estimates depends strongly on corrections for atmospheric effects and an accurate estimate of surface emissivity.
	Radiances received by sensors are influenced by the sensor-viewing angle.
Availability of open-source data.	It is difficult to obtain high spectral, spatial, and temporal resolution with the same instrument.
	A large amount of data exists in various spatial and temporal resolutions, file formats, sizes, and from multiple sources.

Table 1. Benefits and limitations of satellite TIR remote sensing for UHI studies.
(Source: https://appliedsciences.nasa.gov/sites/default/files/2020-11/UHI_Part1_v5.pdf)

Over the last fifty years, the use of satellite TIR data allowed for developing an extensive SUHI research body. Here we present a summary of the main findings together with still controversial aspects:

- **The primary cause of SUHI** is the change in the urban surface energy balance after replacing natural land with artificial surfaces (Arnfield, 2003). SUHI drivers are different, though, during the day and night. A reduction in reflected solar radiation and latent heat flux drives the daytime SUHI. In contrast, the nighttime SUHI is due to larger heat storage during the day, released during the night.
- The formation of SUHIs - and their intensity - **depends on multiple factors**, including climate, population density, city size, landscape structure (materials and distribution), and the level of anthropogenic heat release. The strong interactions among different variables pose serious, multi-collinearity problems that remain poorly understood (Zhou et al., 2019).

4

- **The background climate** is usually considered the ultimate factor that shapes the spatiotemporal differences of SUHIs among cities. In general, the daytime SUHI is larger in humid-hot cities than in their cold-drier counterparts, while the opposite is true during the nighttime (Zhou et al., 2019). The SUHI intensity **differs greatly by season**, being higher in winter than in summer during the night and the opposite during the day for most cities (Zhou, Zhao, Liu, Zhang, & Zhu, 2014). Notice that the formation of cool islands is also possible, like in some arid cities during the summer season in the daytime (Lazzarini, Molini, Marpu, Ouarda, & Ghedira, 2015; Manoli et al., 2019).

- Many studies have used TIR remote sensing to investigate the relationship between **surface characteristics** and SUHI variations. There is a consensus in the literature that land cover/land use and their changes are one of the main causes of UHI formation, driving both urban-rural and intra-urban temperature differences (Deilami, Kamruzzaman, & Liu, 2018). The amount of impervious surface area seems to be the key variable in explaining UHI variation. Increasing the ISA increases the intensity of UHI, whereas the reverse is true for urban vegetation and water bodies (Lu & Weng, 2006; Peng, Xie, Liu, & Ma, 2016). Bare soil areas have ambiguous impacts on SUHI, with studies reporting both positive and negative correlations (Zhou et al., 2019).

- UHI formation depends on not only the landscape composition (material) but also its spatial configuration (distribution). Though it varies among cities, **landscape composition** usually affects the thermal environment more than does spatial configuration (Peng et al., 2016). Still, urban form has a non-negligible impact on SUHI and UHI phenomena (Berger et al., 2017; Yin, Yuan, Lu, Huang, & Liu, 2018). Sensitive urban planning seems to be an effective mitigation strategy (Yin et al., 2018), which requires the management of common urban metrics such as building density, *sky view factor* (SVF), and *floor area ratio* (FAR).

- The **relationship between surface and atmospheric UHIs** has become one of the central topics of SUHI research. This link is not straightforward since both phenomena show opposing behaviors: SUHI peaks during the day in the summer and reaches its minimum at night; the reverse is the case for UHI. Therefore, despite the efforts, the published SUHI-UHI correlations remain empirical (Oke, Mills, Christen, & Voogt, 2017). A leading factor contributing to these uncertainties is that many SUHI analyses rely on very limited datasets (e.g., one image/season or year). The current availability of long-term free data should trigger research using extensive image datasets or time-series to increase the findings' robustness. Another factor is that satellite data only allow for 2D studies, while air temperatures are affected by the complete urban surface (J. a. Voogt & Oke, 1997). Accounting for these three-dimensional effects allows for improving the interpretations of the SUHI magnitude and surface-air temperature differences (Oke et al., 2017).

Despite the substantial advances in SUHI comprehension over the last decades, a recent and exhaustive review on the field revealed that the studies are still strongly biased (Zhou et al. 2019). There are research gaps regarding:

- **Geographic location.** Until now, research has mainly focused on Asia (China), followed by North America (US) and Europe (France, Germany). In contrast, investigations in Central and South America, Africa, and Oceania are still scarce. Due to their high urbanization potentials and/or climate sensitivity, there is a need for more SUHI research in Africa, South America, and India.

- **Time of day.** The majority of the SUHI research concentrated on a single time during daytime, while few night-and-day studies. Data limitation contributes to this research gap in two senses. On the one hand, the most widely used satellite for SUHI detection only has daytime data (i.e., Landsat). On the other, there is a significant missing data problem due to cloud cover.

- **Season.** Over half of the literature focused on the SUHI in an individual season, particularly summer, as the moment when the most intense effects appear. In contrast, few studies investigated the SUHI in all seasons. There is a need for more comprehensive evaluations on day/night SUHIs across different seasons since their intensity and underlying mechanisms vary dramatically through the year. Particularly, nighttime seasonal SUHI patterns remain controversial to date, existing studies reporting more intensive effects in the summer than in the winter and *vice versa*.

- **Research foci.** A central question has been the study of SUHI variability, especially based on ASTER (Baldridge *et al.* 2009) and Landsat data. Most studies have focused on the variations at the local scale rather than at the regional/global scale. Comparisons among cities with similar climates - still scarce compared with intra-urban studies - could help to guide UHI mitigation strategies. Researchers have also investigated the link between SUHI and urban form. However, these studies systematically overlook the 3D nature of cities, being predominant works using satellite TIR data and 2D urban form metrics (Yin et al., 2018).

3. Popularity and scale issues of satellite sensors for urban thermal studies

Urban thermal studies have relied on satellite data from more than ten different onboard sensors (see their main features in Annex 2). To date, the main data providers for thermal urban studies have been, by far, Landsat and MODIS satellites (Zhou et al., 2019). The use of ASTER imagery has been increasing since 2016 (date of free-cost release), and it is now the third most frequent provider. Figure 1 summarizes the reasons for the popularity of these three data sources. Less frequently used satellites are AVHRR, SEVIRI, GOES, HCMM, HJ-1B, AATSR, ITOS-1, COMS, FY-2F, AMSR-E, or AMSR. Notice that temperature data from different satellites may mismatch, due to the differences not only in the sensor features (e.g., viewing angles) but also in the retrieval algorithm and the surface properties (Trigo, Monteiro, Olesen, & Kabsch, 2008).
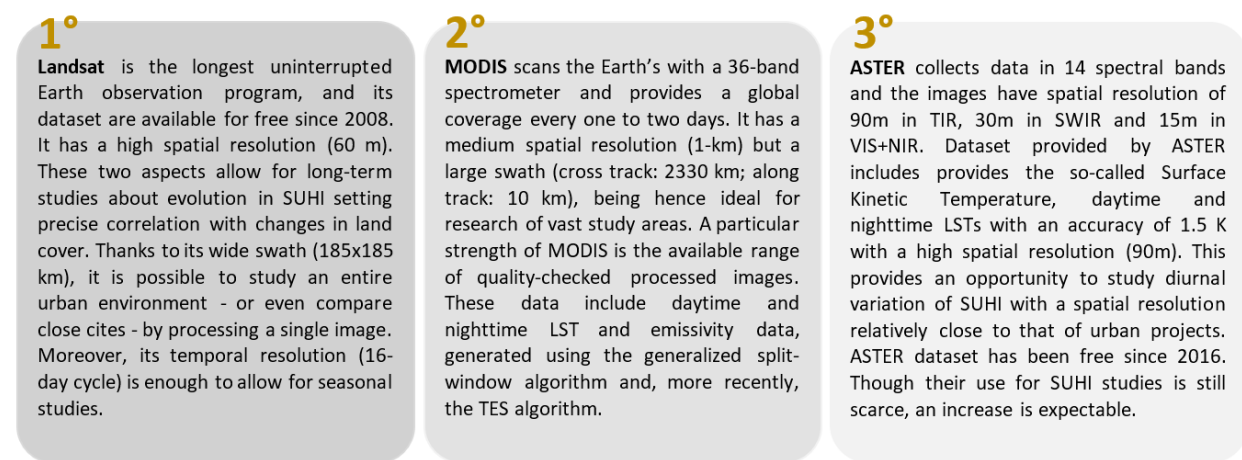
1°

Landsat is the longest uninterrupted Earth observation program, and its dataset are available for free since 2008. It has a high spatial resolution (60 m). These two aspects allow for long-term studies about evolution in SUHI setting precise correlation with changes in land cover. Thanks to its wide swath (185x185 km), it is possible to study an entire urban environment - or even compare close cites - by processing a single image. Moreover, its temporal resolution (16-day cycle) is enough to allow for seasonal studies.

2°

MODIS scans the Earth's with a 36-band spectrometer and provides a global coverage every one to two days. It has a medium spatial resolution (1-km) but a large swath (cross track: 2330 km; along track: 10 km), being hence ideal for research of vast study areas. A particular strength of MODIS is the available range of quality-checked processed images. These data include daytime and nighttime LST and emissivity data, generated using the generalized split-window algorithm and, more recently, the TES algorithm.

3°

ASTER collects data in 14 spectral bands and the images have spatial resolution of 90m in TIR, 30m in SWIR and 15m in VIS+NIR. Dataset provided by ASTER includes provides the so-called Surface Kinetic Temperature, daytime and nighttime LSTs with an accuracy of 1.5 K with a high spatial resolution (90m). This provides an opportunity to study diurnal variation of SUHI with a spatial resolution relatively close to that of urban projects. ASTER dataset has been free since 2016. Though their use for SUHI studies is still scarce, an increase is expectable.

Figure 1. The three most popular sensors for SUHI studies.

Despite the substantial body of knowledge on urban climates developed over the past decades, there is little evidence that this knowledge is incorporated into urban planning and design practice (Mills et al., 2010). Satellite-derived UHI studies are a good example of this issue. To foster the utility of space-based data in the field of urban applications, the European Spatial Agency conducted the project '***Urban heat islands and urban thermography'*** (UHI&UT) between 2008 and 2011. The aim was to develop a set of satellite/airborne-based services to help municipalities to understand and predict UHI phenomena to better prevent/reduce their impacts during summer heatwaves and implement energy efficiency measures. The study involved ten cities, with climates and layouts representative of many urban areas across Europe: Athens, Bari, Brussels, Budapest, Lisbon, London, Madrid, Paris, Seville, and Thessaloniki. For further information on the project, see (Viel, Ceriola, and Ridder 2012).

An original contribution of this work was the **surveys conducted on potential users of urban TIR imagery** from different communities, such as urban engineering departments, civil protection departments, cartography units, meteorological services, local energy, environmental, and sustainability agencies. Users were questioned about applications of TIR they would be interested in and the desirable spatial, temporal, and spectral resolutions required for their purposes. Based on their answers, five application fields emerged (Figure 2a): *Meteorological services, Emergencies, Environmental Quality, Risk analysis, Urban Planning and Energy efficiency*.

a) Users' answers & application fields

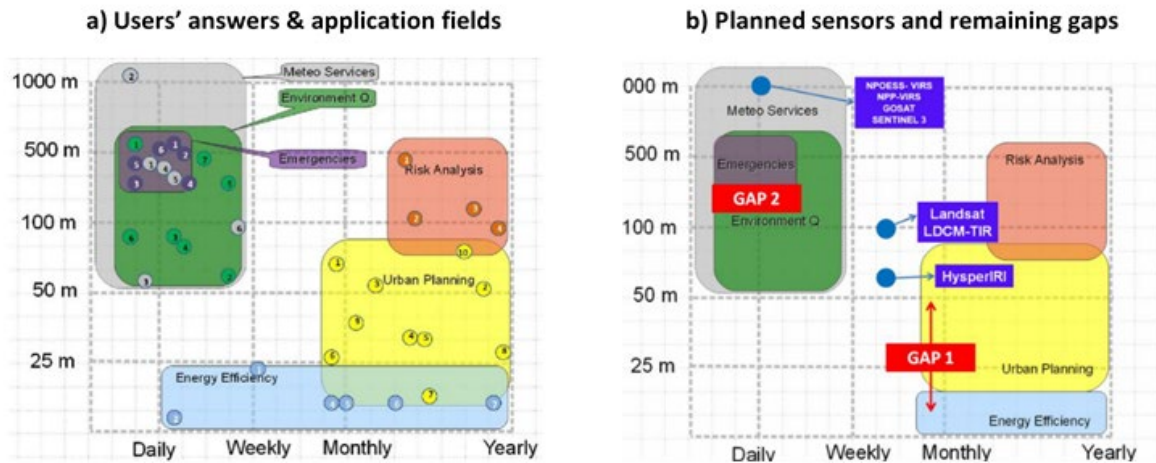**b) Planned sensors and remaining gaps**

Figure 2. Required spatiotemporal resolution of TIR sensors for different application fields (a). Planned sensors (blue dots) and gaps for future devices (red boxes) (b).

Users' answers show that in two fields related to architecture interventions – *energy efficiency* and *urban planning* – the most important parameter is spatial resolution. Imagery products with too coarse spatial resolutions (>30m) make city shapes disappear, and users' observations are hence no longer useful for urban designers (Yin et al., 2018). Figure 3 summarizes the main applications and technical requirements within these two fields.

Energy efficiency

Applications_ Users identified two main applications for thermographies: the detection of roof energy loses to encourage citizens to improve insulation levels; and the analyses of the city network heating systems.

Spatial resolution_ This aspect is the most important one for efficiency purposes. Users reported to need a spatial resolution from 1 m to 50 m, with 15 m as the maximum threshold and 2m as the ideal.

Time resolution_ These studies usually require night and day images to see the variability of the energy fluxes. To study the surfaces behavior, users need, ideally, 2 images a day with the maximum possible amplitude (at least of 6 h).

Spectral requirements_ Sensors needs a spectral resolution between 8-12 µm to ensure a good response in the expected temperature ranges (~25°C- 55°C). The minimum TIR bands for this field are 4 (8.5, 9.0, 9.5 and 10 µm) because the proposed applications require information of materials (e.g., emissivity) that the 4-bands algorithm TES provides. Also, they would need the capacity to react quickly in order to be in good time and conditions.

Urban planning

Applications_ The most demanded products by these users are related to the UHI zoning of the city: UHI intensity, big hot spots, temperature maps in heat waves. The city zoning of the thermal comfort of the citizens is also required. In all the cases, users demand elaborated products matched with other type of information, such as administrative data (e.g., urban block or planning units) or other indicators (e.g., vegetation index, land use or urban morphology).

Spatial resolution_ The hot spot identification requires less than 30 m of spatial resolution and, in general, the zoning of the city demands resolutions of less than 100 m. Comfort analyses require historical series with spatial resolutions between 100-1000 m. At the end, the critical factor remains the ground resolution, ideally ranging between 5 to 100 m.

Time resolution_ The minimum is 1 image per day; the ideal, 2 images per day with the maximum amplitude (> 6 h). The revisit time should be weekly to yearly.

Spectral requirements_ For the Urban Planning field, the temperature range is between 0°C (winter frosts) and 45°C (summer peaks). The recommended option would include a MIR channel (3.7 µm) and two TIR channels (9 and 10.5 µm). The most complete option would include two channels MIR, four channels TIR at least to apply the TES algorithm. Also, it is recommended a band in the red one and another one in the near-infrared, to generate vegetation indexes.

Figure 3. Summary of users' requirements for TIR products in the fields of energy efficiency and urban planning.

8

To ensure simultaneously their utility **for *energy efficiency* and *urban planning* purposes,** satellite sensors should meet the following requirements (Viel, Ceriola, & Ridder, 2012):

- **Spatial resolution**: ideally of 1m, and 15 m at most (Figure 4).
- **Observation time**: 2 images per day with a large amplitude (> 6 h) and a minimal revisit time of a week.
- **Spectral resolution**: 4 TIR bands at least to apply algorithms to retrieve emissivity (8.5/9.0/9.5/10 μm). Ideally, sensors should also include 3 SWIR (1.5/2.1/2.5 μm) and 1 MIR (3.7 μm) bands to provide other products required by the users (e.g., vegetation index) or calculate other algorithms.
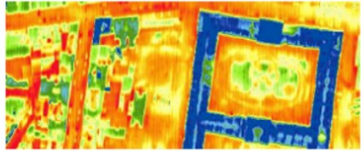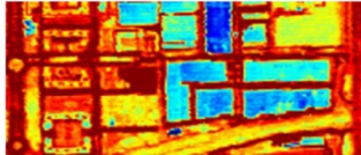

Resolution (m)	Picture
0.5m. With a spatial resolution of 0.5 to 5m it is possible to distinguish neighbourhood/blocks and streets and also buildings. Image source: UHI Winter Thermography	
4 m. There is no big change in visualization between 0.5 to 5m. But from a resolution of 4m, borders of blocks/houses become less net/clear Image source: Desirex08-AHS	
At 15m resolution, streets and blocks are no more distinguishable. This resolution can allow seeing patches of hotter/colder districts. Threshold to still be interesting to be used for energy efficiency purposes. Image source: UHI Winter Thermography	

Figure 4. Example of IR imagery at different spatial resolutions. Source: (Viel et al., 2012)

The UHI&UT project concluded that none of the existing or planned satellite sensors at that time (blue dots) could meet the requirements above. Based on this analysis, this work provided recommendations for future ad-hoc TIR missions and pointed out two priority gaps (red boxes, Figure 2b). Some satellite remote sensing products meet the recommended spatiotemporal resolutions for architectural purposes (e.g., Quick Bird). However, they only cover the visible and near-infrared wavelengths and need to be combined with TIR datasets with coarser resolutions, unavoidably leading to scaling issues (Xu et al., 2017).

Airborne campaigns provide an alternative to overcome the low resolution of satellite thermography. IR cameras on **helicopters or small planes** have been a traditional tool in urban climate studies since the 90s. Voogt and Oke (2003) give a dozen of examples in this regard. More recent iconic campaigns in the urban climate field also chose this option: ESCOMPTE in Marseille (Mestayer et al., 2005), CAPITOUL in Toulouse (Lagouarde et al., 2010; Lagouarde & Irvine, 2008), TOPEUM in Nicosia (Neophytou et al., 2011), and DESIREX in Madrid (J A Sobrino et al., 2009). From these flying altitudes, it is possible to achieve hyperspectral images with spatial resolutions of few meters (~4-10 m) at on-demand temporal resolutions (e.g., twice a day). Though suitable for studying some climatic processes (Lo, Quattrochi, & Luvall, 1997), this imagery is still too coarse for guiding architectural interventions, and repeated aerial flights may be economically unaffordable.

Recent advances in **drones** and radiometric thermal cameras are contributing to overcome these limitations. These technologies make it possible to retrieve urban surface temperatures on-demand at very high spatial resolutions (<1m), with reasonable costs (Gaitani, Burud, Thiis, & Santamouris, 2017; Naughton & McDonald, 2019; Rakha & Gorodetsky, 2018). Combining IR imagery with VIS and NIR data, it is possible to map some physical properties of urban areas, such as NDVI, albedo, *and apparent thermal inertia* (Figure 5). These derived properties may yield valuable information for the decision-making of micro-climatic design and the improvement of urban simulation models (Antoniou, Montazeri, Neophytou, & Blocken, 2019; Fabbri & Costanzo, 2020).
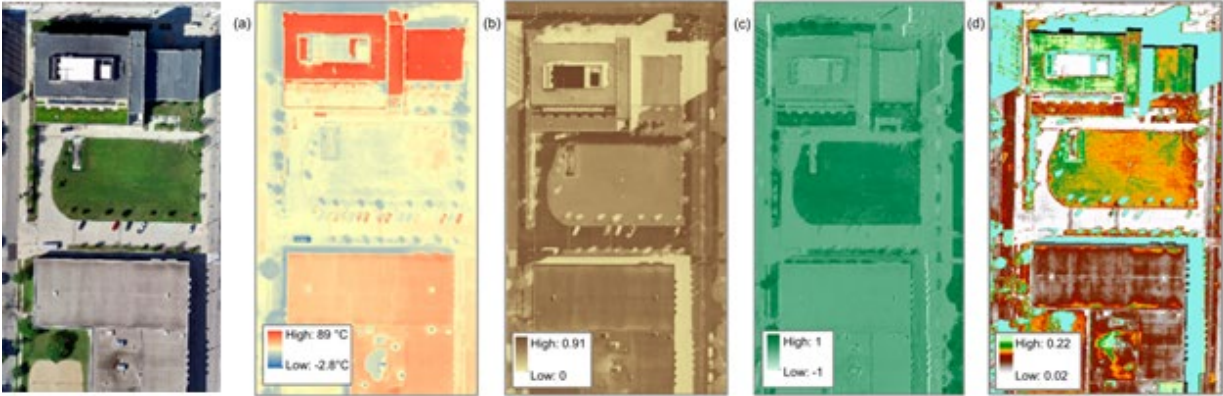

Figure 5. Visual image, surface temperature, albedo, NDVI, and apparent thermal inertia of the urban area surveyed with the drone in (Naughton & McDonald, 2019)*, from left to right.*

4. Attempts to study the true temperature of the 3D urban surface

As such, satellite remote sensing is a two-dimensional source of information about cities. Satellites provide an effective technique to collect extensive thermal data about roofs, roads, water bodies, and other urban horizontal surfaces. In contrast, vertical surfaces, such as façades, are entirely missing in satellite surveys from nadir views or systematically biased from off-nadir sensors (J. A. Voogt & Oke, 1998). The grazing acquisition angles lead to misrepresentations due to the under-sampling of vertical surfaces and the increase of thermal reflections. Another handicap of satellite views are hidden surfaces, masked by other urban elements (e.g., textile or tree canopies).

All these issues remain unsolved in classical airborne studies using airplanes and helicopters. Recently drones have opened up the possibility of sampling both vertical and horizontal surfaces from near frontal views to obtain high-resolution hyperspectral images (Rakha & Gorodetsky, 2018). Thanks to photogrammetric techniques, it is possible to create detailed 3D models incorporating geometrical, optical, and thermal information, like the one in Figure 6. So far, such drone application is only feasible over individual buildings or non-urban areas (e.g., terrains, industrial facilities) due to legal constraints to flights in most cities and other operational problems. Miniaturization of drones and thermal cameras may allow overcoming these limitations in the foreseeable future.
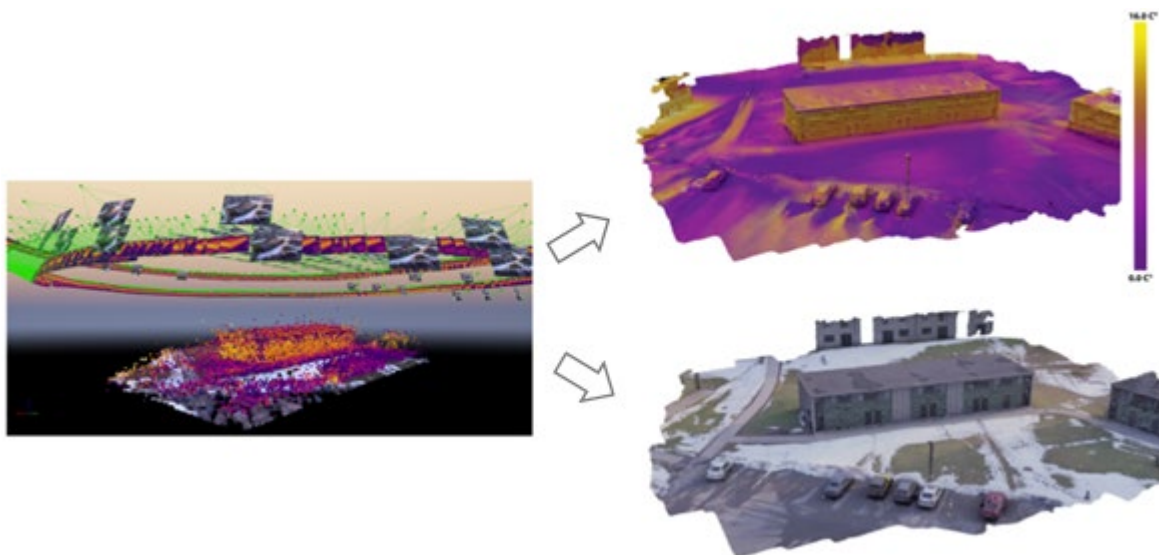

Figure 6. Infrared and RGB models generated using 3D photogrammetry using Pix4D and Rhino3D CAD modeling software. Elaborated from: (Rakha & Gorodetsky, 2018).

As shown, aerial imagery alone cannot provide information about the **temperature of the entire urban skin.** Given the crucial role of this parameter for urban climate at different scales, there have been some attempts to study the *complete urban surface temperatures* over the last two decades.

Early studies opted for the **integration of several datasets collected by different remote sensing devices**. Voogt and Oke (1997) carried out pioneer work by combining airborne observations (nadir and 45° off-nadir) with façade data obtained from vehicle traverses. The significant differences between the complete and airborne estimates of urban surface temperatures during daytime highlighted the need for further research on the subject. Nevertheless, this multi-device approach raised inconsistency issues between datasets due to the difference in resolution, calibration, or device timing (Hartz, Prashad, Hedquist, Golden, & Brazel, 2006).

Later works opted for **perspective views from a single device**, where post-processing and analysis tasks were more intuitive and less time-consuming. The most common method to shoot IR perspectives is to place a thermal camera on the top of **high-rise buildings or tall platforms** (Adderley, Christen, & Voogt, 2015; Christen, Meier, & Scherer, 2012; Chudnovsky, Ben-Dor, & Saaroni, 2004; Ghandehari, Emig, & Aghamohamadnia, 2018; Meier, Scherer, Richters, & Christen, 2011; Morrison, Kotthaus, & Grimmond, 2020; Morrison et al., 2018; Morrison, Yin, et al., 2020; Rotach et al., 2005). Observations from this position typically cover several buildings and their surroundings for several days. The goal is to obtain statistically representative temperatures of the main urban surfaces (roofs, façades, pavements, and tree canopies) at the facet scale. Geographers and climatologists use this information to improve climatic models at the city scale regarding aspects such as:

- The actual density of sensible heat flux released by buildings (Hoyano, Asano, & Kanamaru, 1999)
- The role of thermal admittance and shading history (Meier, Scherer, & Richters, 2010)
- The impact of turbulences on the short-term fluctuation of urban surface temperatures (Christen et al., 2012)

A few studies have used thermography to assess the thermal conditions within urban canyons, crucial for pedestrian comfort and building energy behavior. Due to their complex logistics and the difficulty in selecting representative views, studies at the street level are much scarcer than platform-based investigations. Vehicle transects provide an effective tool to collect data over extensive areas (Asano & Hoyano, 1996; Hilland & Voogt, 2020; J. a. Voogt & Oke, 1997). However, unlike in visible wavelengths, no automated system to conduct drive-by thermography is commercially available yet. In other words, there is no sort of *'Google Street IR View'* (Phan, 2012). Therefore, most of the street-level works rely by now on hand-held cameras (Acuña Paz y Miño, Lawrence, & Beckers, 2020; Boiné, Demers, & Potvin, 2018; Garcia-Nevado, Beckers, & Coch, 2020; Hoyano et al., 1999; S. Lee, Moon, Choi, & Yoon, 2018; Tamura, Hoyano, Hitoshi, & Asano, 2001). The use of rotating devices can help to increase the spatial coverage of the IR camera. This technique allows for generating spherical radiometric maps to describe urban environments (Acuña Paz y Miño et al., 2020; Asano & Hoyano, 1996; Hatefnia, Barakati, Ghobad, & Panah, 2017; Tamura et al., 2001).

The literature review above shows that, over time, the approach of the studies on 3D urban temperatures is evolving. Initially, the focus was on the facet-scale, and the goal was to obtain a statistical thermal sampling of the main urban surfaces, useful for climate models at the city scale (Christen et al., 2012; J. a. Voogt & Oke, 1997). Nowadays, this focus is increasingly on the sub-facet scale to correlate surface temperatures and architecture design (Acuña Paz y Miño et al., 2020; Garcia-Nevado et al., 2020; Hilland & Voogt, 2020; S. Lee et al., 2018; Morrison, Kotthaus, et al., 2020). Recent studies have demonstrated that the architectural details (color, forms) can create significant temperature differences on individual urban facets, particularly on façades (Hilland & Voogt, 2020; Morrison, Kotthaus, et al., 2020) (Figure 7). These findings highlight the importance of sufficiently detailed models to ensure the accuracy of the energy analysis.

-   Figure 7. Map of the mobile traverses (left) carried out in (Hilland & Voogt, 2020) *and example of the visible image (top), thermal image (middle), and classified image (bottom) obtained for a west-facing house.*

5. Algorithms to retrieve surface temperature from satellite sensors

As shown, satellite-based thermography is still too coarse to be useful to guide architectural interventions. However, the algorithms developed to retrieve surface temperature within this field can apply in thermal remote sensing at smaller scales, closer to the architecture domain. After explaining the basics of thermal remote sensing, this section provides an overview of these algorithms, and gives an example of their implementation to an airborne campaign.

5.1 Basics of thermal satellite remote sensing

An infrared sensor onboard a satellite measures all the radiation coming from the land surface and the atmosphere along its line of sight, as illustrated in Figure 8.
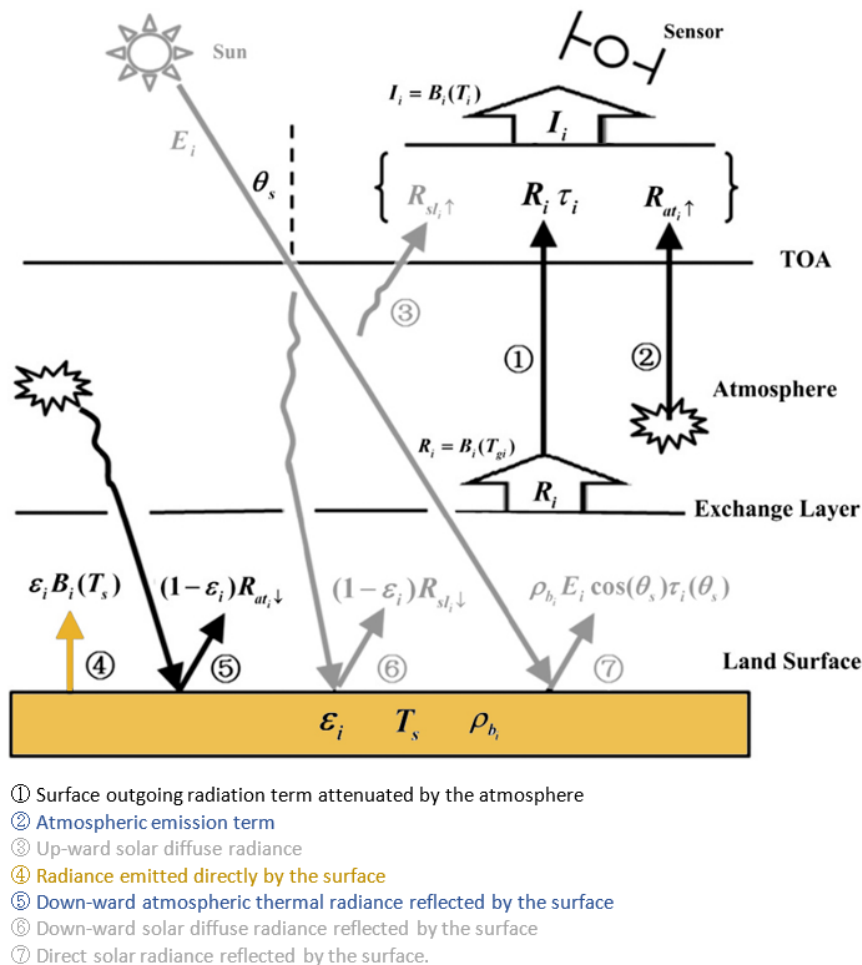

① Surface outgoing radiation term attenuated by the atmosphere
② Atmospheric emission term
③ Up-ward solar diffuse radiance
④ Radiance emitted directly by the surface
⑤ Down-ward atmospheric thermal radiance reflected by the surface
⑥ Down-ward solar diffuse radiance reflected by the surface
⑦ Direct solar radiance reflected by the surface.

Figure 8. Schema of the radiative transfer equation in the infrared wavelength, modified after (Z. L. Li, Tang, et al., 2013).

Based on the radiative transfer equation and assuming a cloud-less atmosphere in thermodynamic equilibrium, the infrared radiance I_i received by the sensor at the top of the atmosphere (TOA) in a certain channel i from a particular view direction (θ, φ) can be written as (Eq. 1):

$$I_i \;=\; \underbrace{R_i(\theta, \varphi)\tau_i(\theta, \varphi)}_{①} \;+\; \underbrace{R_{at_i}\!\uparrow(\theta, \varphi)}_{②} \;+\; \underbrace{R_{sl_i}\!\uparrow(\theta, \varphi)}_{③}$$

The at-sensor radiance is the sum of three terms...

Surface outgoing radiation term attenuated *by the atmosphere*

Atmospheric emission term

Solar diffusion term

The outgoing radiation from the land surface R_i comprises not only the radiation emitted by the surface itself but also the radiation coming from the sun and the atmosphere and reflected by it (Eq. 2):

$$R_i = \underbrace{\varepsilon_i(\theta,\varphi)\, B_i(T_s)}_{\substack{④ \\ \textit{Radiance} \\ \textit{emitted by the} \\ \textit{surface}}} + \underbrace{[1-\varepsilon_i(\theta,\varphi)]\, R_{at_i\downarrow}}_{\substack{⑤ \\ \textit{Down-ward radiance} \\ \textit{emitted by the atmosphere} \\ \textit{and reflected by the surface}}} + \underbrace{[1-\varepsilon_i(\theta,\varphi)]\, R_{sl_i\downarrow}}_{\substack{⑥ \\ \textit{Down-ward diffuse solar} \\ \textit{radiance reflected by the} \\ \textit{surface}}} + \underbrace{E_i\cos\theta_s\,\tau_i(\theta_s,\varphi_s)\rho_{b_i}(\theta,\varphi,\theta_s,\varphi_s)}_{\substack{⑦ \\ \textit{Direct solar radiance, transmitted} \\ \textit{by the atmosphere, and reflected} \\ \textit{by the surface}}}$$

in which τ_i is the effective transmittance of the atmosphere; ε_i and ρ_{b_i} are the emissivity and bi-directional reflectivity of the surface; $B_i(T_s)$ is the spectral radiance of a black-body surface at a temperature T_s; $R_{at_i\downarrow}$ and $R_{at_i\uparrow}$ are the down and up-welling thermal radiance of the atmosphere; $R_{sl_i\downarrow}$ and $R_{sl_i\uparrow}$ are the down and up-welling solar diffuse radiance resulting from atmospheric scattering of the solar radiance; E_i is the solar irradiance at the TOA and θ_s and φ_s are the solar zenithal and azimuthal angles.

As the contribution of solar radiation at the TOA (E_i) in the 8–14 µm window during both day and night and in the 3–5 µm window at night is negligible, we can disregard the terms ③, ⑥, ⑦ in the expressions above without loss of accuracy (Z. L. Li, Tang, et al., 2013). By doing so, we can reformulate the at-sensor radiance as follows (Eq.3):

$$I_i = \underbrace{\varepsilon_i(\theta,\varphi)\, B_i(T_s)\,\tau_i(\theta,\varphi)}_{\substack{\textit{Radiance emitted by the} \\ \textit{surface and attenuated by the} \\ \textit{atmosphere}}} + \underbrace{[1-\varepsilon_i(\theta,\varphi)]\, R_{at_i\downarrow}\,\tau_i(\theta,\varphi)}_{\substack{\textit{Radiance emitted by the atmosphere,} \\ \textit{reflected by the surface and attenuated} \\ \textit{by the atmosphere}}} + \underbrace{R_{at_i\uparrow}(\theta,\varphi)}_{\substack{\textit{Radiance emitted} \\ \textit{by the atmosphere}}}$$

The at-sensor radiance is the sum of three terms…

Once $B_i(T_s)$ is derived from Eq. 3, the inversion of the Planck's law allows for retrieving the surface temperature as follows (Eq.4):

$$T_s = \frac{c_2}{\ln\left[\dfrac{c_1 + \lambda^5 B_i(T_s)}{\lambda^5 B_i(T_s)}\right]^\lambda}$$

Planck's law inversion (Eq. 4)
Where c_1 and c_2 are two radiant constants of value:
$c_1 = 2\pi hc^2 = 3{,}741832 \times 10^{-16}$ W m^{-2} K^{-4}; $c_2 = \frac{hc}{k} = 1{,}438786 \times 10^{-2}$ m K.
Being: c=299.792.458 m s^{-1}, is the speed of light in the vacuum; h=6,626176 ×10^{-34} W s^2, is the Planck constant; k = 1,380662×10^{-23} W s K^{-1}, is the Boltzmann constant.

The main problem in the T_s retrieval lies in the fact that the simultaneous determination of these two parameters from space is not possible using a passive radiometer alone because the number of unknowns to be determined is always larger than the number of the independent measurements (Z. Li, Petitcolin, & Zhang, 2000). Satellite sensors measure radiance at N wavelengths. Therefore, there will always N equations but N + 1 unknowns, corresponding to the N emissivities (one at each wavelength) and an unknown surface temperature. In other words, the surface temperature retrieval requires simultaneous retrieval of the surface emissivity and *vice versa*.

Several algorithms have been proposed to solve this undetermined problem by reducing the unknowns based on different assumptions (José A. Sobrino & Jiménez-Muñoz, 2005). These satellite algorithms can be grouped into two families: those requiring *a priori* knowledge of the surface emissivity (*Section 5.2*) and those that do not (*Section 5.3*). Li et al. provided a comprehensive review of the main algorithms in each family (Z. L. Li, Tang, et al., 2013). Here we present just a summary of these methods, highlighting those aspects useful for field works at other scales.

5.2. Retrieval with known emissivity

If the emissivity is known, the retrieval of the surface temperature is possible by three kind of methods: single-channel, multi-channel, and multi-angle methods. Table 2 summarizes the main features of these algorithms.

Single-channel methods

Single-channel methods retrieve surface temperature by applying *Equation 1* to the radiance measured by the satellite sensor in a **single channel** (around 10 µm) after correcting the atmospheric effects (attenuation, scattering and self-emission). The best wavelength depends on the atmospheric water vapor, and varies from 11 µm to 10.5 µm when the water vapor varies from 1 g/cm² to 4 g/cm² (José A. Sobrino & Jiménez-Muñoz, 2005).

Several radiative transfer models are available to simulate such effects (e.g., MODTRAN, LOWTRAN). They necessitate **accurate information of atmospheric profiles** at the satellite overpass, an almost impossible requirement to meet in most cases. Approximations are possible from ground-based radio soundings, satellite vertical soundings or meteorological forecasting models. The latter option seems to provide the better compromise in terms of accuracy and spatial coverage of data. Alternative approaches derive this data from empirical correlations with near-surface measurements.

Example from (José A. Sobrino & Jiménez-Muñoz, 2005)*:

$$T_s = T_i + \frac{(1-\varepsilon_i)}{\varepsilon_i}\{L_i(T_i) - (1-\tau_i)[T_a + L_i(T_i) - T_i]\} + \frac{(1-\tau_i)}{\varepsilon_i \tau_i}$$

Where T_a is the atmospheric temperature; $L_i(T_i)$ is a parameter given by:

$$L_i(T_i) = \frac{B_i(T_i)}{\left[\frac{\partial B_i(T)}{\partial T}\right]_{T_i}}$$

* For a generalized single-channel algorithm, see (Jiménez-Munoz & Sobrino, 2003)

Multi-channel method

Multichannel methods retrieve surface temperature by applying *Equation* 1 to **two channels** located in the thermal spectral range (~ from 10 to 12 µm). The so-called split-window algorithms (SW) retrieve LST using a linear or non-linear combination of the top-of-atmosphere (TOA) brightness temperatures from two different channels (e.g., 10 and 12.5 µm). These methods utilize the differential atmospheric absorption in several adjacent channels to obtain LST data without information about the atmospheric profiles at the time of the acquisition. Each specific method defines their own coefficients a_n to parametrize aspects such as the total column water vapor in the atmosphere (WV) and the viewing zenith angle (VZA).

Algorithms using three or more TIR channels are also available. Some of them include also MIR channel to improve atmospheric corrections during nighttime. Increasing the number of channels may increase the accuracy of the method, but it comes with the expense of increased measurement error due to instrumental noise and emissivity uncertainties in other bands. Notice that the range of emissivity values and their uncertainty for natural or man-made surfaces is significantly higher for MIR and 8.7 µm channels than for the most commonly used SW channels (Trigo, Peres, DaCamara, & Freitas, 2008).

Example of linear SW (Z. L. Li, Tang, et al., 2013): $\quad T_s = a_0 + a_1 T_i + a_2(T_i - T_j)$

where a_n are coefficients that depend on the spectral response function of the two channels $g_i(\lambda)$ and $g_j(\lambda)$, the emissivity in the two channels, the WV and the VZA; T_i and T_j are the brightness temperatures measured in the two channels.

Multi-angle method

Similar to the split-window method, the multi-angle method is based on differential atmospheric absorption when the same object is observed from different viewing angles due to the different path-lengths. Accurate geometric registrations between images are crucial for this method. It does not need an accurate profile of atmospheric profiles, but it requires a priori knowledge on the angular variations of materials, not always available.

Example from (Z. L. Li, Tang, et al., 2013):

$$T_s = T_n + p_1(T_n - T_f) + p_2 + p_3(1 - \varepsilon_n) + p_4(\varepsilon_n - \varepsilon_f)$$

Where T_n and T_f are the brightness temperatures measured in the nadir and forward views; ε_n and ε_f are the emissivity in these two directions; p_n are coefficients related to the atmospheric transmittances and mean equivalent air temperatures in the two views.

Table 2. Methods to retrieve surface temperature with known emissivity.

In practice, the optimal method depends on the characteristics of the sensor, the availability (and reliability) of emissivity and atmospheric data, the complexity of the approach, and other considerations. For instance, multi-angle methods are only applicable when IR imagery is simultaneously available from two different views, a piece of information only provided by few satellite sensors, such as the ATSR (existing) or the SPECTRA (planned).

When comparing the three methods with known emissivity, Sobrino and Jiménez-Muñoz (2005) concluded that:

- Single-channel methods provide similar - or even better - results with low atmospheric water vapor contents than split-window and dual-angle algorithms.
- On a global scale, split-window and dual-angle algorithms provide better results than single-channel methods because the latter performs poorly with high water vapor contents.
- Dual-angle algorithms have slightly better results than split-window, though they have two major operational drawbacks: (1) the angular dependence of emissivity is not well-known (2) they need a good registration between the nadir and forward pixels.

Objects observed under different angles may exhibit different temperatures due to the three-dimensional nature of land surfaces, making registration impossible over complex surfaces. Therefore, multi-angle methods are only suitable for homogeneous areas (e.g., sea surface) under ideal atmospheric (i.e., without clouds).

5.3. Retrieval with unknown emissivity

In practice, the heterogeneity of the surface and the angular and spectral variation of the LSE makes it challenging to accurately determine the emissivity at the satellite pixel scale in advance. Over time, **three approaches to retrieve LST if the emissivity is not known appeared:** stepwise retrieval, simultaneous LST and LSE retrieval methods with known atmospheric information, and simultaneous retrieval of LST, LSEs, and atmospheric profiles (Table 3).

Stepwise retrieval methods

In the stepwise retrieval methods, the emissivity is determined in the first place, and then the LST is estimated using any of the previous methods. There are two alternatives to estimate emissivity.

The first is determining the emissivity (semi-)empirically from VNIR measurements that help to classify surfaces into classes with known emissivity values. For example, in the **classification-based emissivity method** (CBEM), surfaces are classed into land cover types; in the **NDVI-based method**, into soil types. Notice that the accuracy of these approaches depends on the accuracy in the classification and on the knowledge of the emissivity values associated to each class.

The second alternative to estimate emissivity is the use of pairs of atmospherically corrected MIR and TIR radiances at ground level. This is the approach taken in the **day/night TISI-based method** (Becker & Li, 1990). This technique calculates temperature-independent spectral-indices (TISI) for the TIR and MIR channels, and estimates emissivity assuming that these indices should remain constant over time. This method performs better than the two previously mentioned. However, it requires day & night data observed under similar observation conditions, as well as accurate image co-registration and atmospheric corrections in MIR and TIR channels.

Simultaneous retrieval of LST and ε with known atmospheric data

If the atmospheric information is available, it is possible to retrieve LST and LSE simultaneously by increasing the temporal or spectral data available to reduce the unknowns or increase the number of equations.

The multi-temporal methods use measurements at different times assuming that the spectral emissivity is time-invariant. The two main methods in this category are the **two-temperature method (TTM)** (Watson, 1992), which uses one channel, and the **physics-based day/night operational method (D/N)**, which uses MIR and TIR channels.

In the multi-spectral methods, the assumption concerns the intrinsic spectral behavior of emissivity. For example, the **gray body emissivity method (GBE)** assumes that the emissivity has a flat spectrum in a certain interval, usually for wavelengths larger than 10 µm (Z. L. Li, Wu, et al., 2013); while the **temperature emissivity separation (TES)** method assumes that there is a spectral contrast in emissivity (Alan Gillespie et al., 1998; AR Gillespie, Rokugawa, Hook, Matsunaga, & Kahle, 1999). With the popularization of hyperspectral sensors, the TES algorithm has become one of the most widespread methods. See its requirements and limitations in Annex 2.

A simplified version of the GBE model (Artis & Carnahan, 1982): $\varepsilon = exp\big(\alpha(T_j - T_i) \,/\, T_j T_i(\lambda_j - \lambda_i)\big)$

Where T_i and T_j are the brightness temperatures measured in the two channels, with wavelength λ_i and λ_j; α is a constant involving the Planck's (h) and Boltzmann's (K) constants and the speed of light (c): $\alpha = hc/K$ $(1.438 \times 10^{-2}\ mK)$.

Simultaneous retrieval of LST, ε and atmospheric profiles

Finally, it is also possible to retrieve surface temperature with unknown emissivity and atmospheric data. These new methods take advantage on the narrow bandwidth offered by hyperspectral TIR sensors with thousands of channels. The representatives of these methods are the artificial neural network (ANN) method (Wang et al., 2010) and the two-step physical retrieval method (Ma et al., 2002, 2000). These methods are more complex to perform and their results, harder to interpret.

Table 3. Methods to retrieve surface temperature with unknown emissivity.

A possible contribution of the previous satellite algorithms could be an adaptation of the CBE methods to image-segmentation of ground-based thermography, currently done manually or by surface orientation. For satellite datasets, the TISI and TES methods seem to exhibit slightly better behavior than the others (Z. L. Li, Wu, et al., 2013). An adaptation of the GBE method could be also interesting, but it could be troublesome in the some metallic and non-metallic materials (Kotthaus, Smith, Wooster, & Grimmond, 2014). In any case, to test the potential of these methods in ground-based observations, these should provide multispectral thermal data (instead of single broadband measurements).

5.4. Applying satellite algorithms to airborne TIR campaigns: the DESIREX example

Methods to retrieve surface temperature with unknown emissivities are commonly used in satellite-based studies. In contrast, these techniques are seldom implemented in studies at smaller scales, except for some punctual airborne-based studies. This is the case of the DESIREX campaign described below.

The **D**ual-use **E**uropean **S**ecurity **IR EX**periment (DESIREX) was a measurement campaign of the European Space Agency conducted in Madrid between June 23 and July 6, 2008. The aim was to generate thermal datasets as input to the TIR sensor to address upcoming trade-off studies (e.g., *The Urban Heat Islands and Urban Thermography Project,* or UHI&UT). The campaign included airborne and ground-based hyperspectral measurements and atmospheric data (Ta, RH, radiosondes). The airborne sensor was an 80-band AHS radiometer, which covers the visible and near-infrared (VNIR), shortwave infrared (SWIR), mid-infrared (MIR), and thermal infrared (TIR) ranges. The ground-based sensor was a radiance-based radiometer with 6 TIR bands between 8–13 μm.

Within the framework of this project, Oltra-Carrió et al. (2012) compared three different methodologies to retrieve urban surface emissivity: the NDVI thresholds method, the temperature-and-emissivity separation (TES) algorithm, and the temperature-independent spectral indices (TISI) algorithm. Additionally, they used local data at four sites to assess the performance of these methods (Figure 9).
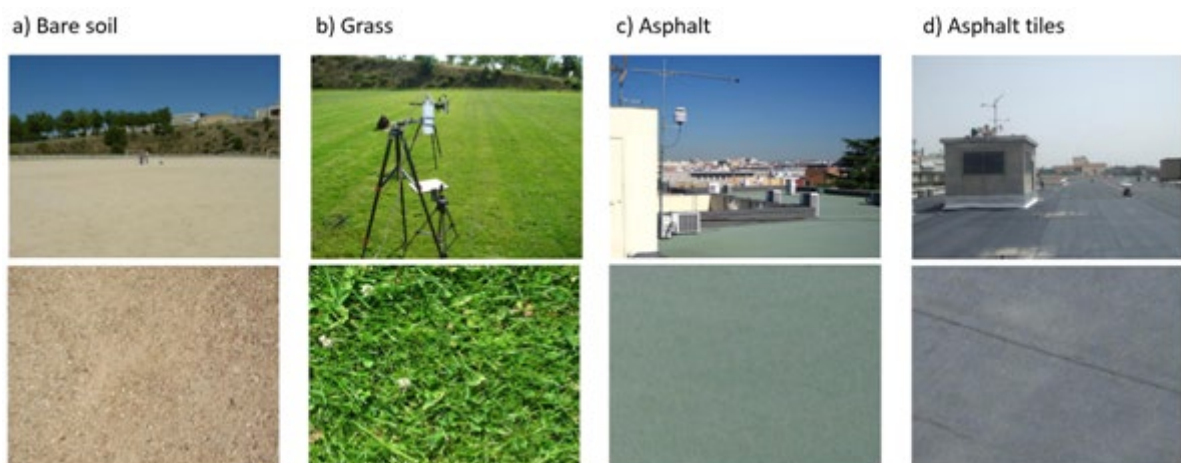

Figure 9. Detailed and general views of the sites selected for validation of airborne data against ground-based measurements in the DESIREX campaign [Elaborated from: (Oltra-Carrió et al., 2012)].

Over artificial urban surfaces, TES and TISI showed better agreement with in-situ data than NDVI. TES algorithm reproduces better LST over the studied area without needing high temporal resolution of the sensor. However, TES algorithms fail over certain kinds of surfaces, particularly metallic ones.

Sobrino et al. (2012) proposed an alternative to overcome this limitation of the TES method by combining it with a classification-based approach (CBEM). First, urban surfaces are classed into categories. Then, the TES algorithm is applied to those classes where the algorithm provides satisfactory results (see Annex 2). Finally, values extracted from spectral libraries (http://speclib.jpl.nasa.gov) are assigned to the rest of the classes. Notice that the selected ε-spectra may be somewhat arbitrary since spectral libraries include "representative" samples, while surfaces over the city can be highly variable. Based on this hybrid method, Sobrino's team could generate an emissivity map of an extensive urban area of Madrid (Figure 10).
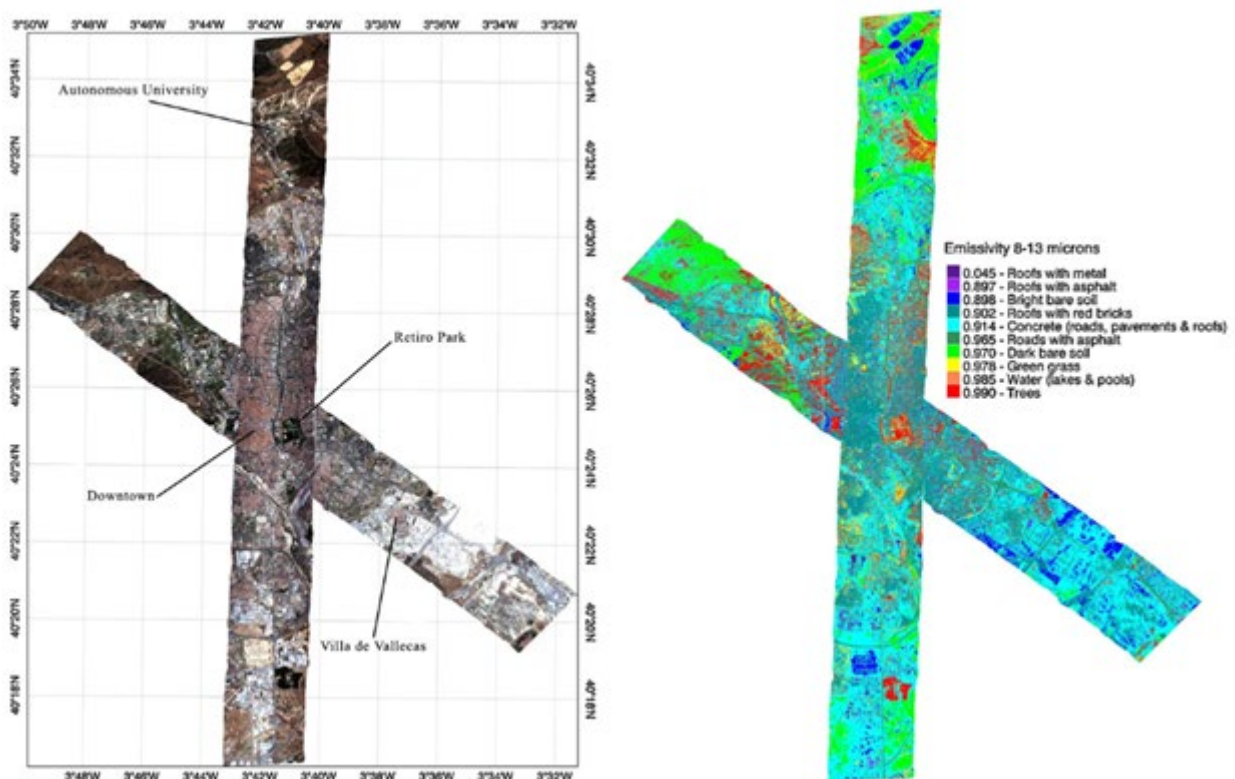

Figure 10. AHS imagery of Madrid on 4 July 2008 at 11:30 GMT (left) and emissivity map using the classification-based approach between 8 and 13 μm (right). Elaborated from: (J. A. Sobrino et al., 2012)*.*

The DESIREX campaign highlighted the crucial impact of emissivity on the accuracy of the retrieved surface temperature. Sobrino *et al*. reported that the difference in surface temperature obtained from corrected and un-corrected emissivity data was up to 4 K (J. A. Sobrino et al., 2012). Oltra-Carrió *et al*. show differences of up to 3 K depending on the method used to retrieve emissivity (Oltra-Carrió et al., 2012).

6. From satellite to ground-based thermography corrections

Two types of corrections are necessary to retrieve the *actual* surface temperatures (T_s) from remote sensing data. The first correction aims to remove the **atmospheric effects;** the second aims to account for the **emissivity effects.** Though common in satellite studies, such tasks are not routinely applied in ground-based TIR imagery. Satellite T_s retrieval procedures are not directly applicable because of the unique challenges posed by perspective views over complex urban geometries (Hammerle, Meier, Heinl, Egger, & Leitinger, 2017)(Morrison, Yin, et al., 2020).

Unlike in satellite studies, the distances between the sensor and the different parts of the scene (Z_{path}) may significantly vary in ground-based imagery, so do the **atmospheric effects**. Corrections treating Z_{path} as a constant can result in over or underestimations of surface temperature. These errors can be non-negligible because atmospheric correction can be significant over relatively short path lengths (e.g., up to 3 K in 155 m (Morrison, Yin, et al., 2020)). Atmospheric effects are particularly noticeable with large differences in surface-to-air temperature, a typical situation in urban environments during the day (Meier et al., 2011; J. A. Voogt & Oke, 2003). The use of 3D models and computer vision techniques allows for more accurate Z_{path} computation that makes it possible pixel-by-pixel atmospheric corrections using radiative models such as MODTRAN (Meier et al., 2011; Morrison, Yin, et al., 2020).

The **emissivity-related corrections** involve quantifying two aspects: the **emissivity** and the **reflected radiance** across the observed surfaces. These tasks differ between satellite and ground-based remote sensing:

- Satellite-based studies usually use **emissivities** obtained using a per-pixel approach (i.e., effective emissivity). In contrast, ground-based observations require a *per-object* approach (Yang, 2011). Ground-based studies usually classify surfaces and associate an emissivity value to each class manually, a time-consuming task. Therefore, studies tend to oversimplify the number of classes, even assigning a single emissivity for the entire scene. In reality, the emissivity of urban surfaces can be highly variable (Kotthaus et al., 2014). Moreover, the existing spectral libraries[1] do not adequately cover the immense diversity of urban materials, particularly in metals (Figure 11). Automatic classification algorithms and methods to retrieve T_s without a priori knowledge of emissivity are available for satellite/airborne remote sensing (*Section 5.3*), but they are not for ground-based studies.
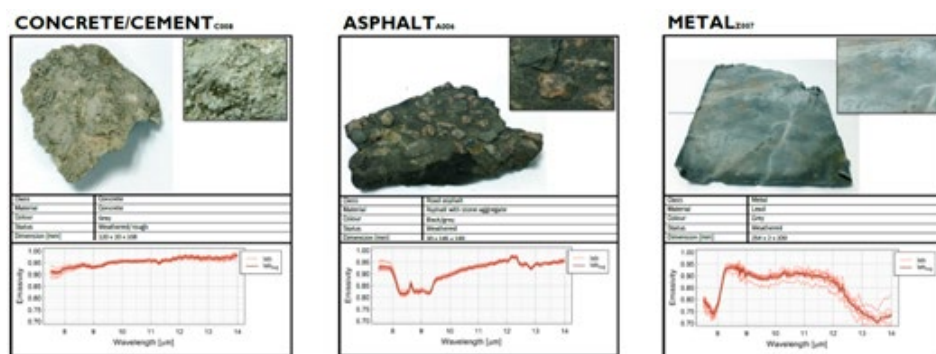

Figure 11. Spectral emissivity of three impervious urban materials. Source: (Kotthaus et al., 2014).

---

[1] Two reference spectral libraries are **ASTER** (Baldridge, Hook, Grove, & Rivera, 2009) (https://speclib.jpl.nasa.gov/) and **SLUM** (Kotthaus et al., 2014) (https://urban-meteorology-reading.github.io/SLUM). The latter work provides data from 74 samples collected using field-portable spectrometers in controlled laboratory conditions with methodologies applicable to outdoors.

- **The radiation reflected by urban surfaces** sensor may come from the sky vault and other urban surfaces. Satellite RS corrections usually do not account for the second contribution based on the assumption that at the pixel scale the land is approximately a flat surface (see Eq.3 from *Section 5.1*). At the typical ground-based RS scales, urban geometry is an important influence on scattered radiation from the sky and canopy elements (Figure 12).
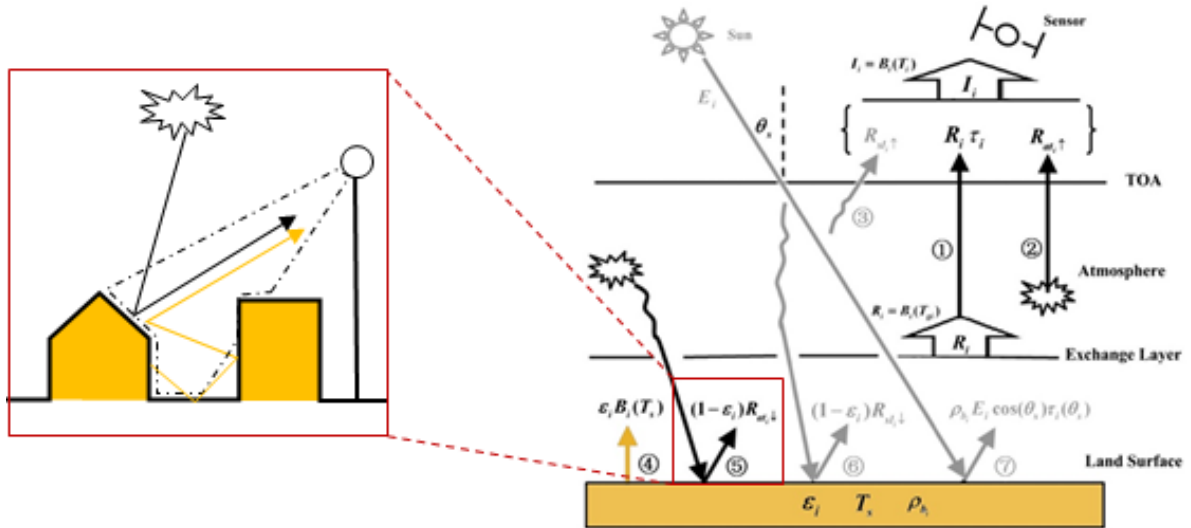

Figure 12. Modeling of the radiation reflected by urban surfaces in ground-based (left) vs satellite observations (right) modified after (Z. L. Li, Tang, et al., 2013) .

Given the complexity of these scattering processes, many studies opt for assuming that all surfaces behave as black-bodies, working in terms of *brightness temperatures* (Christen et al., 2012; Garcia-Nevado et al., 2020; J. a. Voogt & Oke, 1997). Some airborne and ground-based studies have used the Sky View Factor (SVF) to approximate the multiple scattering of radiation in urban geometries, as exemplified in Eq.5 (Adderley et al., 2015):

$$R_{reflected} \uparrow = (1 - \varepsilon_i) \left[SVF \, R_{at_i\downarrow} + (1 - SVF) \, \sigma \, T_{env}^4 \right] \quad \text{(Eq. 5)}$$

These approaches assume that all surfaces are Lambertian, atmospheric irradiance is isotropic ($R_{at_i\downarrow}$), and the surrounding urban facets all have a uniform surface temperature (T_{env}), equal to the air o the average brightness temperature of the surroundings. The isothermal assumptions for the sky and surroundings introduce uncertainties that could be larger than the ones due to the choice in material emissivity (up to 0.3K), as shown in (Morrison, Yin, et al., 2020). The explicit consideration of thermal reflections, very rare in ground-based thermography (Morrison, Yin, et al., 2020), requires solving the complete heat transfer problem between the urban surfaces and the sky.

All in all, most of the ground-based TIR studies typically neglect atmospheric effects on their observations (Morrison, Kotthaus, et al., 2020), except for Meier's works (Meier, 2011).To our best knowledge, only one ground-based study has accounted for both the atmospheric and emissivity corrections in detail over a complex urban geometry (Morrison, Yin, et al., 2020). This work exploits the capabilities of the *Discrete Anisotropic Radiative Transfer Model* (DART), released in 1996 and updated since then by Gastellu-Etchegorry's team (Gastellu-Etchegorry, Grau, & Lauret, 2012). DART allows for simulating 3D radiative transfer processes from visible to thermal infrared wavelengths in

natural and urban landscapes using a ray-tracing approach ("DART," n.d.). The prerequisite to run simulations is the availability of a 3D urban model discretized into voxels. In this case, photogrammetric techniques were used on Google Earth imagery to create a highly detailed urban model that includes vegetation and buildings. Figure 13 illustrates the impact of the pixel-by-pixel correction of atmospheric and emissivity effects on T_s.
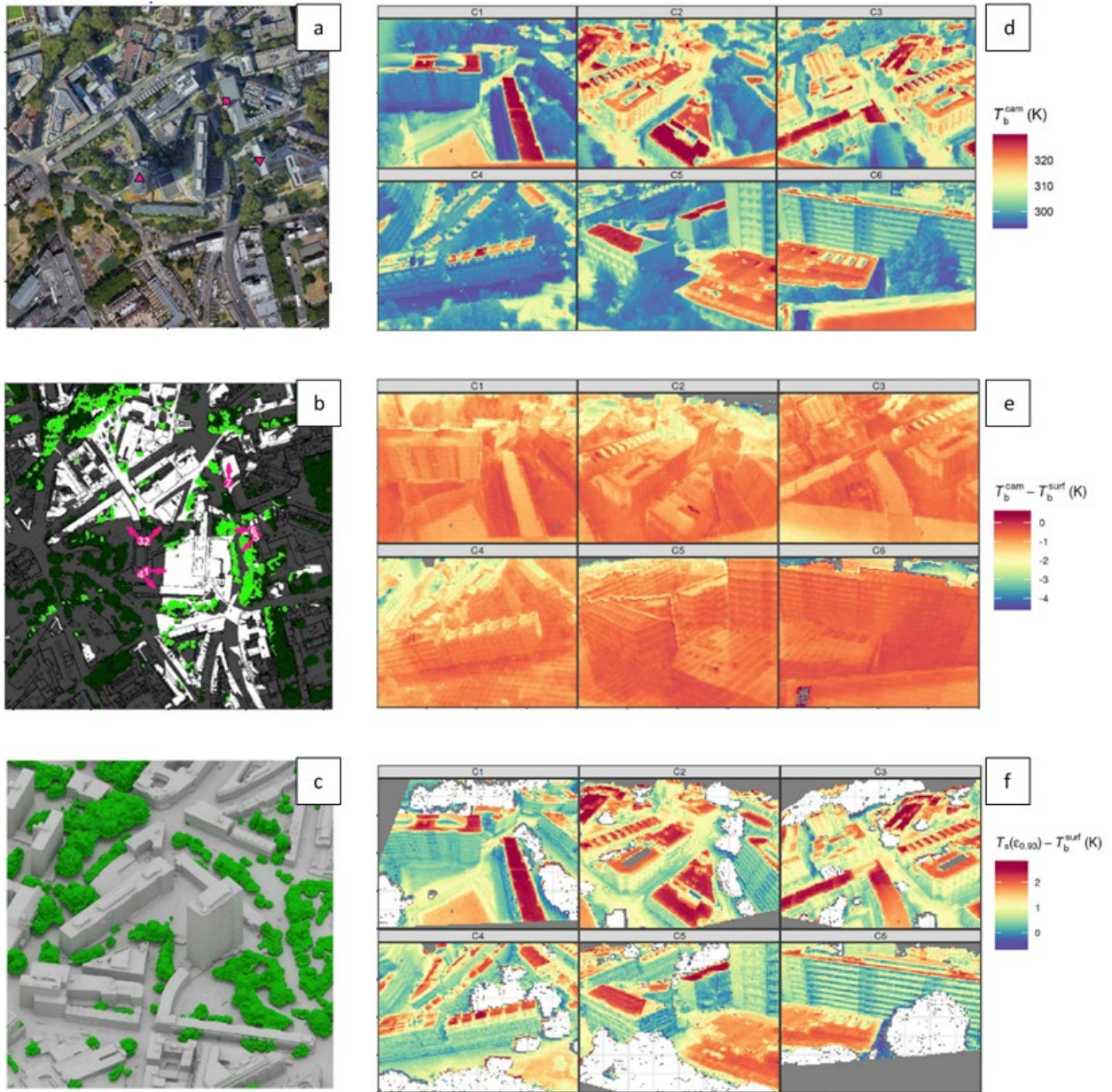

Figure 13. Ortoimage of the study site, aerial and detailed views of the corresponding urban model (a, b, c) in (Morrison, Kotthaus, et al., 2020; Morrison, Yin, et al., 2020).
Brightness temperatures from the six thermal cameras before corrections, T_b^{cam} (d).
Difference in brightness temperatures before and after the atmospherical corrections, T_b^{surf} (e).
Difference in temperatures before and after the emissivity corrections for ε=0.93, $T_s^{ε=0.93}$ (f)

7. Challenges for future ground-based thermal remote sensing

Corrected ground-based thermography has potential applications in different fields, namely: the estimation of complete urban surface temperatures, the evaluation of building and urban energy balance models, ground-truthing of airborne or space-borne measurements, the assessment of the directional anisotropy of LWIR radiation, simulation calibrations within urban projects, and development of urban material databases. The full exploitation of the possibilities of this remote sensing approach requires addressing three challenges:

- **Re-definition of measurement protocols.** Ground-based thermography usually consists of measurements in a single broad waveband, typically between 7 and 14 μm. A shift towards TIR imagery in several narrow wavebands (e.g., 4 TIR channels) would allow the adaptation of the satellite algorithms to retrieve ε and T_s simultaneously to the context of ground-based measurements (e.g., TES-like algorithms). Another critical issue is the suitable measurement timing to find a trade-off between data availability and post-processing requirements. The requirements of multi-temporal methods could offer a guide in this regard (*Section 5*), but day and night data are both necessary. Also, there are technical issues to solve, such as the calibration and housing of longwave infrared cameras for outdoor settings (Morrison, Yin, et al., 2020).

- **Emissivity-related issues.** Research on the angular emissivity behavior has focused on natural surfaces (i.e., water, ice, crops) rather than on artificial materials, dominant in urban settlements. Observations from towers and platforms may provide consistent TIR multi-angle datasets to address this question. In addition, multi-reflections within concave geometries can result in an effective increase in emissivity (Peeters, Ribbens, Dirckx, & Steenackers, 2016). More studies at the street level in the line of (Beckers & Garcia-Nevado, 2019) are necessary to investigate these effects in some urban forms, such as narrow urban canyons. Another open question concerns the degree of specularity of urban materials in IR wavelengths (from SWIR to LWIR). Specular thermal reflections over glass surfaces are evident, and their modeling can be critical in curve geometries ("Walkie Talkie architect 'didn't realise it was going to be so hot,'" 2013). However, their role in other common urban materials is still unclear. By now, the common practice is to consider all surfaces as Lambertian thermal emitters, even though directional modeling and measure are technically possible ("DART," n.d.; Ianiro & Cardone, 2010). Another worth-exploring path is the need for increasing the number of thermal bands considered in thermal simulations. This subject requires further research on the spectral behavior of urban materials (Kotthaus et al., 2014).

- **Increase in the level of detail of the urban model**. As shown in this report, the most significant advances in ground-based thermography correction were possible thanks to the combination of complementary radiative simulations and highly detailed geometrical models (Meier et al., 2011; Morrison, Yin, et al., 2020). In contrast, simplistic models are still the norm in urban climate studies, despite the fact the computational limitations of the past are now vanishing (e.g., Figure 14). As observations can be made of the complete 3D urban skin, a description of the material composition of the vertical surfaces is particularly important. The first step would be the differentiation of glasses from opaque surfaces. If glass emissivity is unaccounted for, wall temperatures may be overestimated in ground observations (Morrison, Yin, et al., 2020). Also, sidewalks affected by glass reflections

can be hotter than the others by several degrees [up to 4.7 ∘C in (Naughton & McDonald, 2019)]. An option to increase the model semantics would be using reconstruction techniques that incorporate automatic window detection (Lee and Nevatia 2004). Since reconstructed models are usually hard to manage and edit (Aliaga, 2013), procedural modeling could be an alternative that would also bring the possibility of simulating non-existing scenarios.
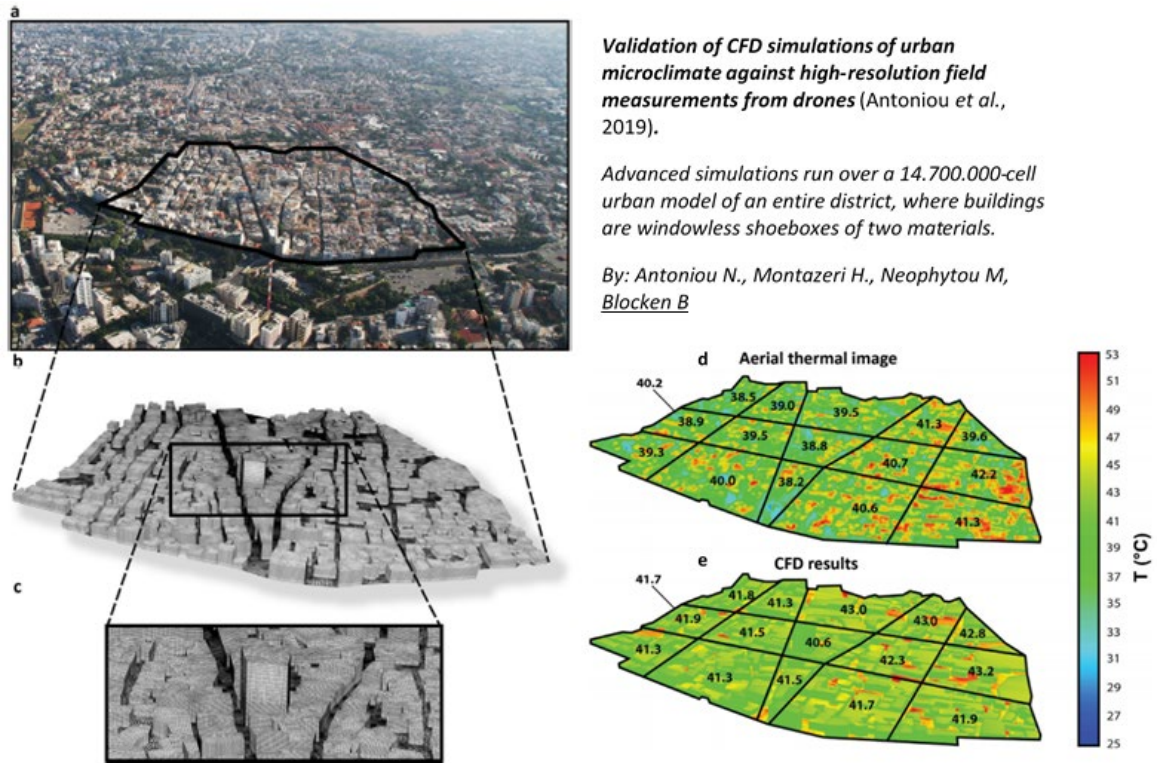

Figure 14. Aerial view of the case study area (a) and corresponding computational grid (b, c) in (Antoniou et al., 2019). Aerial thermography vs CFD simulation results (e, f).

8. Conclusion

Thermal remote sensing has played a central role in urban climate studies, especially in the Urban Heat Island domain. Since the '70s, an astonishing number of papers using thermal remote sensing from satellite sensors appeared. In comparison, studies relying on airborne and, even more, ground-based thermography are far more limited.

Satellite-based thermal studies are rarely applicable to architectural interventions. The first reason is that their temporal and spatial resolutions do not match those concerning the architecture scale. The coarse resolution of satellite sensors allows for assessing some dynamics of urban climates, such as detecting spatial thermal patterns related to changes in land cover due to urbanization. However, project decision-making requires knowledge about the thermal responses of individual building components, only possible with higher resolution sensors. The revisit times and spatial resolutions of thermal data from aircrafts such as helicopters and airplanes, though an improvement, seem to remain insufficient for architectural purposes. Drone and ground-based remote sensing are potentially more suitable in this sense. Also, these close-by observations help to overcome the second drawback of satellite-datasets for architectural purposes: the lack of information about façades. This report shows that these two remote sensing approaches are still in their infancy compared to the satellite domain: few studies, excessive manual work, and poor spectral resolution.

Regardless of the chosen approach, atmospheric and emissivity corrections are necessary to retrieve surface temperatures from remote sensing data. How to perform these corrections in urban ground-based IR imagery remains an open question insofar. This report shows that the availability of 3D urban models with the appropriate geometric and semantic level of detail is crucial for this purpose.

A highly detailed geometry allows for accurate path-length computations, increasing this way the accuracy of atmospheric corrections. Also, it allows for accurate computations of view factors among surfaces (instead of SVF-based proxies) that improve the corrections of the reflected radiation calculated with radiative models (e.g., DART). Up until now, the major obstacle for ground-based observations is the individual assignment of emissivities to the observed surfaces. The practice that prevails is setting one single emissivity for the entire model, disregarding any directional effect. These shortcomings are not due to technical issues or lack of physical models (algorithms for the visual wavelengths are available) but to the lack the input data.

In this context, a rethink of the satellite methods to retrieve surface temperature with unknown emissivity could be of particular interest. Some of these algorithms were already tested on airborne datasets with promising results. We found no examples during this review of their implementation on ground-based observations (usually based on observations in a single broad waveband between 8-14 μm). Hyperspectral high-resolution imagery yields the potential for detailed and comprehensive mapping of urban surface materials. However, new measurement protocols for ground-based thermography are necessary.

ANNEX 1: Summary of TIR sensors and satellites.

Satellite	Orbit	Swath	Temporal Coverage	Free since...	Sensor	(Name)	Spectral Bands (µm)	Spatial Resolution	Temporal Resolution	Satellite Radiance Data Access	Land Surface Temperature Data Products
Landsat 4[a] Landsat 5 Landsat 7 Landsat 8	Polar (10 am/pm)	185 km	7/1982 -12/1993 3/1984 - 01/2013 4/1999 - Present 02/2013 - Present	2008	TM ETM+ TIRS OLI	Thematic Mapper Enhanced Thematic Mapper Thermal Infrared Sensor [b]Operational Land Imager	10.40 - 12.50 10.40 - 12.50 10.6 - 11.19 11.50 - 12.51	120 m (30 m resampled) 60 m (30 m) 100 m 100 m	16 days	https://earthexplorer.usgs.gov/	https://www.usgs.gov/media/files/landsat-provisional-surface-temperature-product-guide
Terra & Aqua	Polar: (Terra & Aqua) 10:30 & 1:30 am/pm	2330 km	12/1999 - Present 04/2002 - Present	2002?	MODIS	MODerate-resolution Imaging Spectroradiometer Advanced	10.78 - 11.28 11.77 - 12.27	1 km	12 hours	https://modis.gsfc.nasa.gov/tools/	https://modis.gsfc.nasa.gov/data/dataprod/mod21.php
Terra	10:30 am/pm	60 km	12/1999 - Present	2016	ASTER	Advanced Spaceborne Thermal Emission and Reflection Radiometer	10.25 - 10.95 10.95 - 11.65	90 m	12 hours	https://lpdaac.usgs.gov/products/ast_09tv003/	https://lpdaac.usgs.gov/products/ast_08v003/
International Space Station/ ECOsystem Spaceborne Thermal Radiometer Experiment on Space Station (ECOSTRESS)	Varying	385 to 415 km	06/2018 - Present		PHyTIR	Prototype HyspIRI Thermal Infrared Radiometer	8.28, 8.79, 9.06, 10.5, 12.05	60 m CONUS only	varies/ every few days	https://ecostress.jpl.nasa.gov/data	https://lpdaac.usgs.gov/products/eco2lstev001/
*Suomi National Polar Partnership (NSPP) Joint Polar Satellite System-1 (NOAA 20)	Polar, 1:30 am/pm	3000 km	10/2011 - Present 11/2018 - Present		VIIRS	Visible Infrared Imaging Radiometer Suite	10.26 - 11.26 11.54 - 12.49	750 m	12 hours	https://ladsweb.modaps.eosdis.nasa.gov/	https://viirsland.gsfc.nasa.gov/Products/NASA/LSTESDR.html
NOAA Operational Series Current: NOAA 15,18,19 ESA- Metop-A & B	Polar, 2:00 am/pm	2900 km	1979 - Present		AVHRR	Advance Very High-Resolution Radiometer	10.30 - 11.30 11.5 - 12.50	1 km & 4 km		https://www.ncdc.noaa.gov/cdr/fundamental/avhrr-radiances-nasa	
NOAA Geostationary Operational Environmental Satellites (GOES) Current: GOES-16 & GOES-17	Geostationary 10-min Image Updates		1975 - Present		VISSR ABI	Advance Baseline Imager	10.10 - 10.60 10.80 - 11.60 11.80 -12.80 13.0 - 13.6	2 km CONUS and Full Disk	minutes, hours, day/night	https://www.bou.class.noaa.gov/saa/products/search?datatype_family=GRABIPRD	https://www.avl.class.noaa.gov/saa/products/search?datatype_family=GRABIPRD
ESA - Sentinel 3A & 3B	Polar, 10 am/pm	> 740 km	02/2016 - Present 04/2018 - Present		SLSTR	Sea and Land Surface Temperature Radiometer	10.45 - 11.24 11.57 - 12.48	1 km	12 hours	https://scihub.copernicus.eu/dhus/#/home	
ESA - Sentinel 2A & 2B	Polar, 10:30 am/pm	290 km	07/2015 - Present 03/2017 - Present		MSI	[c]MultiSpectral Instrument					

[a] Landsats 1, 2, and 3 had a Multi Spectral Scanner that did not have thermal IR bands. [b] Used for land cover/NDVI/impermeable surface. [c] Used for land cover. In gray, data with potential application for urban interventions.
Satellite Radiance and Derived Products Data Search (Source: https://appliedsciences.nasa.gov/sites/default/files/2020-11/UHI_Part1_v5.pdf)
Other sources of: https://earthdata.nasa.gov/ |||| https://earthexplorer.usgs.gov/

ANNEX 2: Comments on the TES algorithm and its accuracy

The Temperature and Emissivity Separation (TES) algorithm was originally developed to provide with high accuracy LST (±1.5 K) and ε (±0.015) information from satellite data (Alan Gillespie et al., 1998). Nevertheless, this approach is also applicable to ground-based measurements acquired with thermal multiband radiometers (J. A. Sobrino et al., 2012).

This method starts from an initial emissivity guess for all pixels and channels and uses an empirical relationship that allows estimating the minimum emissivity of the spectrum by taking into account the spectral contrast, thus to obtain the emissivity for all channels (Oltra Carrió, 2013).

The TES algorithm is composed by three modules (AR Gillespie et al., 1999): NEM (Normalized Emissivity Method), RATIO and MMD (Maximum–Minimum Difference). The NEM module includes an iterative procedure which provides a first guess for LST/ε from atmospherically corrected thermal radiance, sky irradiance and an initial value of ε based on the radiative transfer equation. The RATIO module obtains relative emissivities by rationing the NEM emissivities to their average value. Finally, the MMD module scales the emissivity spectra in order to provide the final values for LST and ε.

The key part of TES algorithm is the MMD module. It relies on an empirical relationship between spectral contrast (MMD) and minimum emissivity (ε_{min}) determined from laboratory and/or field emissivity spectra according to the following expression: $\varepsilon_{min} = a + b \times MMD^c$. Accordingly, the TES algorithm provide satisfactory results only over surfaces with ε spectra that meet this ε_{min}– MMD relationship. This is not the case of surfaces with low spectral contrast, such as water and green vegetation.

The following figure depicts the ε_{min}–MMD relationship over manmade materials to assess the performance of TES algorithm over urban areas. It can be seen that abundant urban surfaces, such as concrete or asphalt, meet this relationship. Therefore, accurate results are expectable over these materials when applying the TES algorithm. However, some artificial surfaces, mainly highly reflective metals, do not follow the ε_{min}–MMD relationship and, thus, TES algorithm will not provide satisfactory results. There are other methodologies to obtain land surface parameters of these materials (e.g., Malaplate et al. (2001) using information from 3 μm to 5 μm and alternate measurements under sun and shade.
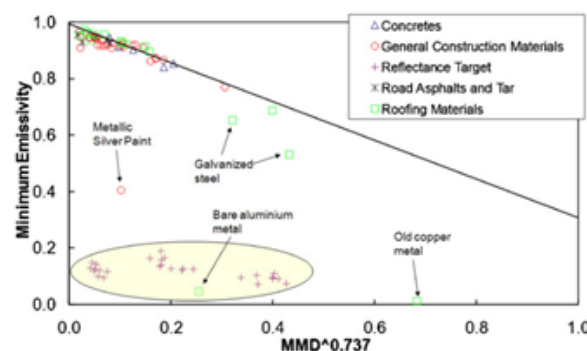

Fig. 4. Plot of minimum emissivity (emin) versus spectral contrast (MMD) for spectra of man-made materials included in the ASTER spectral library. The line given by $\varepsilon_{min} = 0.994 - 0.687 MMD^{0.737}$ (original expression of TES algorithm) is also represented.

Figure 15. Source: (J. A. Sobrino et al., 2012)

REFERENCES

Acuña Paz y Miño, J., Lawrence, C., & Beckers, B. (2020). Visual metering of the urban radiative environment through 4π imagery. *Infrared Physics and Technology*, *110*(August), 103463. https://doi.org/10.1016/j.infrared.2020.103463

Adderley, C., Christen, A., & Voogt, J. A. (2015). The effect of radiometer placement and view on inferred directional and hemispheric radiometric temperatures of an urban canopy. *Atmospheric Measurement Techniques*, *8*(7), 2699–2714. https://doi.org/10.5194/amt-8-2699-2015

Aliaga, D. G. (2013). Geometrical Models of the City. In Benoit Beckers (Ed.), *Chapter 9. Solar Energy at Urban Scale* (pp. 191–203). Wiley.

Antoniou, N., Montazeri, H., Neophytou, M., & Blocken, B. (2019). CFD simulation of urban microclimate: Validation using high-resolution field measurements. *Science of the Total Environment*, *695*, 133743. https://doi.org/10.1016/j.scitotenv.2019.133743

Arnfield, J. (2003). Two decades of urban climate research: A review of turbulence, exchanges of energy and water, and the urban heat island. *International Journal of Climatology*, *23*(1), 1–26. https://doi.org/10.1002/joc.859

Artis, D. A., & Carnahan, W. H. (1982). Survey of emissivity variability in thermography of urban areas. *Remote Sensing of Environment*, *12*(4), 313–329. https://doi.org/10.1016/0034-4257(82)90043-8

Asano, K., & Hoyano, A. (1996). Development of an urban thermal environment measurement system using a new spherical thermography technique. *Proceedings of SPIE Conference on Thermosense*, *2744*.

Baldridge, A. M., Hook, S. J., Grove, C. I., & Rivera, G. (2009). The ASTER spectral library version 2.0. *Remote Sensing of Environment*, *113*(4), 711–715. https://doi.org/10.1016/j.rse.2008.11.007

Becker, F., & Li, Z. L. (1990). Temperature-independent spectral indices in thermal infrared bands. *Remote Sensing of Environment*, *32*(1), 17–33. https://doi.org/10.1016/0034-4257(90)90095-4

Beckers, B., & Garcia-Nevado, E. (2019). Urban Planning Enriched by Its Representations, from Perspective to Thermography. In A. Sayigh (Ed.), *Sustainable Vernacular Architecture.* (pp. 165–180). https://doi.org/10.1007/978-3-030-06185-2_9

Berger, C., Rosentreter, J., Voltersen, M., Baumgart, C., Schmullius, C., & Hese, S. (2017). Spatio-temporal analysis of the relationship between 2D/3D urban site characteristics and land surface temperature. *Remote Sensing of Environment*, *193*, 225–243. https://doi.org/10.1016/j.rse.2017.02.020

Boiné, K., Demers, C. M. H., & Potvin, A. (2018). Spatio-temporal promenades as representations of urban atmospheres. *Sustainable Cities and Society*. https://doi.org/10.1016/j.scs.2018.04.028

Christen, A., Meier, F., & Scherer, D. (2012). High-frequency fluctuations of surface temperatures in an urban environment. *Theoretical and Applied Climatology*, *108*(1–2), 301–324. https://doi.org/10.1007/s00704-011-0521-x

Chudnovsky, A., Ben-Dor, E., & Saaroni, H. (2004). Diurnal thermal behavior of selected urban objects using remote sensing measurements. *Energy and Buildings*, *36*(11), 1063–1074. https://doi.org/10.1016/j.enbuild.2004.01.052

DART. (n.d.). Retrieved November 30, 2020, from The Discrete Anisotropic Radiative Transfer Model website: https://dart.omp.eu/#/

Deilami, K., Kamruzzaman, M., & Liu, Y. (2018). Urban heat island effect: A systematic review of spatio-temporal factors, data, methods, and mitigation measures. *International Journal of Applied Earth Observation and Geoinformation*, *67*(December 2017), 30–42. https://doi.org/10.1016/j.jag.2017.12.009

Fabbri, K., & Costanzo, V. (2020). Drone-assisted infrared thermography for calibration of outdoor microclimate simulation models. *Sustainable Cities and Society*, *52*(May 2019), 101855. https://doi.org/10.1016/j.scs.2019.101855

Gaitani, N., Burud, I., Thiis, T., & Santamouris, M. (2017). High-resolution spectral mapping of urban thermal properties with Unmanned Aerial Vehicles. *Building and Environment*, *121*, 215–224. https://doi.org/10.1016/j.buildenv.2017.05.027

Garcia-Nevado, E., Beckers, B., & Coch, H. (2020). Assessing the cooling effect of urban textile shading devices through time-lapse thermography. *Sustainable Cities and Society*, *63*, 102458. https://doi.org/10.1016/j.scs.2020.102458

Gastellu-Etchegorry, J. P., Grau, E., & Lauret, N. (2012). DART : A 3D Model for Remote Sensing Images and Radiative Budget of Earth Surfaces. In C. Alexandru (Ed.), *Modeling and Simulation in Engineering*.

Ghandehari, M., Emig, T., & Aghamohamadnia, M. (2018). Surface temperatures in New York City: Geospatial data enables the accurate prediction of radiative heat transfer. *Scientific Reports*, *8*(1), 1–10. https://doi.org/10.1038/s41598-018-19846-5

Gillespie, Alan, Rokugawa, S., Matsunaga, T., Steven Cothern, J., Hook, S., & Kahle, A. B. (1998). A temperature and emissivity separation algorithm for advanced spaceborne thermal emission and reflection radiometer (ASTER) images. *IEEE Transactions on Geoscience and Remote Sensing*, *36*(4), 1113–1126. https://doi.org/10.1109/36.700995

Gillespie, AR, Rokugawa, S., Hook, S. J., Matsunaga, R., & Kahle, A. B. (1999). Temperature/emissivity separation algorithm theoretical basis document, version 2.4. In *Nasa/Gsfc*. Retrieved from http://eospso.gsfc.nasa.gov/sites/default/files/atbd/atbd-ast-05-08.pdf

Hammerle, A., Meier, F., Heinl, M., Egger, A., & Leitinger, G. (2017). Implications of atmospheric conditions for analysis of surface temperature variability derived from landscape-scale thermography. *International Journal of Biometeorology*, *61*(4), 575–588. https://doi.org/10.1007/s00484-016-1234-8

Hartz, D. A., Prashad, L., Hedquist, B. C., Golden, J., & Brazel, A. J. (2006). *Linking satellite images and hand-held infrared thermography to observed neighborhood climate conditions*. *104*, 190–200. https://doi.org/10.1016/j.rse.2005.12.019

Hatefnia, N., Barakati, A., Ghobad, M., & Panah, A. E. (2017). Reliable methodology to monitor and assess radiant environments. *Proceedings of 33rd PLEA International Conference: Design to Thrive, PLEA 2017*, *1*(July), 1092–1099.

Hilland, R. V. J., & Voogt, J. A. (2020). The effect of sub-facet scale surface structure on wall brightness temperatures at multiple scales. *Theoretical and Applied Climatology*, *140*(1–2), 767–785. https://doi.org/10.1007/s00704-020-03094-7

Hoyano, A., Asano, K., & Kanamaru, T. (1999). Analysis of the sensible heat flux from the exterior surface of buildings using time sequential thermography. *Atmospheric Environment*, *33*(24–25), 3941–3951. https://doi.org/10.1016/S1352-2310(99)00136-3

Ianiro, A., & Cardone, G. (2010). Measurement of surface temperature and emissivity with stereo dual-wavelength IR thermography. *Journal of Modern Optics*, *57*(18), 1708–1715. https://doi.org/10.1080/09500340.2010.514068

Jiménez-Munoz, J. C., & Sobrino, J. A. (2003). A generalized single-channel method for retrieving land surface temperature from remote sensing data. *Journal of Geophysical Research: Atmospheres*, *108*(22). https://doi.org/10.1029/2003jd003480

Kotthaus, S., Smith, T. E. L., Wooster, M. ., & Grimmond, C. S. B. (2014). Derivation of an urban materials spectral library through emittance and reflectance spectroscopy. *ISPRS Journal of Photogrammetry and Remote Sensing*, *94*, 194–212. https://doi.org/10.1016/j.isprsjprs.2014.05.005

Lagouarde, J. P., Hénon, A., Kurz, B., Moreau, P., Irvine, M., Voogt, J., & Mestayer, P. (2010). Modelling daytime thermal infrared directional anisotropy over Toulouse city centre. *Remote Sensing of Environment*, *114*(1), 87–105. https://doi.org/10.1016/j.rse.2009.08.012

Lagouarde, J. P., & Irvine, M. (2008). Directional anisotropy in thermal infrared measurements over Toulouse city centre during the CAPITOUL measurement campaigns: First results. *Meteorology and Atmospheric Physics*, *102*(3–4), 173–185. https://doi.org/10.1007/s00703-008-0325-4

Lazzarini, M., Molini, A., Marpu, P. R., Ouarda, T. B. M. J., & Ghedira, H. (2015). Urban climate modifications in hot desert cities: The role of land cover, local climate, and seasonality. *Geophysical Research Letters*, *42*(22), 9980–9989. https://doi.org/10.1002/2015GL066534

Lee, S. C., & Nevatia, R. (2004). Extraction and integration of window in a 3D building model from ground view images. *Proceedings of the IEEE Computer Society Conference on Computer Vision and Pattern Recognition*, *2*(January 2004). https://doi.org/10.1109/cvpr.2004.1315152

Lee, S., Moon, H., Choi, Y., & Yoon, D. K. (2018). Analyzing Thermal Characteristics of Urban Streets Using a Thermal Imaging Camera: A Case Study on Commercial Streets in Seoul, Korea. *Sustainability*, *10*(2), 519. https://doi.org/10.3390/su10020519

Li, Z. L., Tang, B. H., Wu, H., Ren, H., Yan, G., Wan, Z., Trigo, I. F., Sobrino, J. A. (2013). Satellite-derived land surface temperature: Current status and perspectives. *Remote Sensing of Environment*, *131*, 14–37. https://doi.org/10.1016/j.rse.2012.12.008

Li, Z. L., Wu, H., Wang, N., Qiu, S., Sobrino, J. A., Wan, Z., Tang, B. H., Yan, G. (2013). Land surface emissivity retrieval from satellite data. *International Journal of Remote Sensing*, *34*(9–10), 3084–3127. https://doi.org/10.1080/01431161.2012.716540

Li, Z., Petitcolin, F., & Zhang, R. (2000). A physically based algorithm for land surface emissivity retrieval from combined mid-infrared and thermal infrared data. *Science in China, Series E: Technological Sciences*, *43*(SUPPL.), 32–33. https://doi.org/10.1007/bf02916575

Lo, C. P., Quattrochi, D. a, & Luvall, J. C. (1997). Application of high-resolution thermal infrared remote sensing and GIS to assess the urban heat island effect. *International Journal of Remote Sensing*, *18*(2), 287–304.

Lu, D., & Weng, Q. (2006). Spectral mixture analysis of ASTER images for examining the relationship between urban thermal features and biophysical descriptors in Indianapolis, Indiana, USA. *Remote Sensing of Environment*, *104*(2), 157–167. https://doi.org/10.1016/j.rse.2005.11.015

Manoli, G., Fatichi, S., Schläpfer, M., Yu, K., Crowther, T. W., Meili, N., Burlando, P., Katul, G. G., Bou-Zeid, E. (2019). Magnitude of urban heat islands largely explained by climate and population. *Nature*, *573*(7772), 55–60. https://doi.org/10.1038/s41586-019-1512-9

Meier, F. (2011). *Thermal remote sensing of urban microclimates by means of time-sequential thermography* (Ph.D. Thesis). Technischen Universität Berlin.

Meier, F., Scherer, D., & Richters, J. (2010). Determination of persistence effects in spatio-temporal patterns of upward long-wave radiation flux density from an urban courtyard by means of Time-Sequential Thermography. *Remote Sensing of Environment*, *114*(1), 21–34. https://doi.org/10.1016/j.rse.2009.08.002

Meier, F., Scherer, D., Richters, J., & Christen, A. (2011). Atmospheric correction of thermal-infrared imagery of the 3D urban environment acquired in oblique viewing geometry. *Atmospheric Measurement Techniques*, *4*(5), 909–922. https://doi.org/10.5194/amt-4-909-2011

Mestayer, P. G., Durand, P., Augustin, P., Bastin, S., Bonnefond, J. M., Bénech, B., Campistron, B., Coppalle, A., Delbarre, H., Dousset, B., Drobinski, P., Druilhet, A., Fréjafon, E., Grimmond, C. S.B., Groleau, D., Irvine, M., Kergomard, C., Kermadi, S., Lagouarde, J. P., Lemonsu, A., Lohou, F., Long, N., Masson, V., Moppert, C., Noilhan, J., Offerle, B., Oke, T. R., Pigeon, G., Puygrenier, V., Roberts, S., Rosant, J. M., Sanïd, F., Salmond, J., Talbaut, M.,Voogt, J. (2005). The urban boundary-layer field campaign in Marseille (UBL/CLU-ESCOMPTE): Set-up and first results. *Boundary-Layer Meteorology*, *114*(2), 315–365. https://doi.org/10.1007/s10546-004-9241-4

Mills, G., Cleugh, H., Emmanuel, R., Endlicher, W., Erell, E., McGranahan, G., Ng, E., Nickson, A., Rosenthal, J., Steemer, K. (2010). Climate information for improved planning and management of mega cities (Needs Perspective). *Procedia Environmental Sciences*, *1*(1), 228–246. https://doi.org/10.1016/j.proenv.2010.09.015

Morrison, W., Kotthaus, S., & Grimmond, C. S. B. (2020). Urban surface temperature observations from ground-based thermography: intra- and inter-facet variability. *Urban Climate*, *35*(November 2020), 100748. https://doi.org/10.1016/j.uclim.2020.100748

Morrison, W., Kotthaus, S., Grimmond, C. S. B., Inagaki, A., Yin, T., Gastellu-etchegorry, J., Kanda, M., Merchant, C. J., Lw, C. M. (2018). A novel method to obtain three-dimensional urban surface temperature from ground-based thermography. *Remote Sensing of Environment*, *215*(May), 268–283. https://doi.org/10.1016/j.rse.2018.05.004

Morrison, W., Yin, T., Lauret, N., Guilleux, J., Kotthaus, S., Gastellu-etchegorry, J., Norford, L., Grimmond, S. (2020). Atmospheric and emissivity corrections for ground-based thermography using 3D radiative transfer modelling. *Remote Sensing of Environment*, *237*(March 2019), 111524. https://doi.org/10.1016/j.rse.2019.111524

Naughton, J., & McDonald, W. (2019). Evaluating the variability of urban land surface temperatures using drone observations. *Remote Sensing*, *11*(14). https://doi.org/10.3390/rs11141722

Neophytou, M., Fokaides, P., Panagiotou, I., Ioannou, I., Petrou, M., Sandberg, M., Wigo, H., Linden, E., Ivanov, A. (2011). Towards Optimization of Urban Planning and Architectural Parameters for Energy use Minimization in Mediterranean Cities. *Proceedings of the World Renewable Energy Congress – Sweden, 8–13 May, 2011*, *57*, 3372–3379. https://doi.org/10.3384/ecp110573372

Oke, T. R., Mills, G., Christen, A., & Voogt, J. A. (2017). *Urban Climates*. Columbia: Cambridge University Press.

Oltra-Carrió, R., Sobrino, J. A., Franch, B., & Nerry, F. (2012). Land surface emissivity retrieval from airborne sensor over urban areas. *Remote Sensing of Environment*, *123*, 298–305. https://doi.org/10.1016/j.rse.2012.03.007

Oltra Carrió, R. C. (2013). Thermal remote sensing of urban areas. The case study of the urban heat island of Madrid. Univ. Politecnica de Valencia.

Peeters, J., Ribbens, B., Dirckx, J. J. J., & Steenackers, G. (2016). Determining directional emissivity: Numerical estimation and experimental validation by using infrared thermography. *Infrared Physics and Technology*, *77*, 344–350. https://doi.org/10.1016/j.infrared.2016.06.016

Peng, J., Xie, P., Liu, Y., & Ma, J. (2016). Urban thermal environment dynamics and associated landscape pattern factors: A case study in the Beijing metropolitan region. *Remote Sensing of Environment*, *173*, 145–155. https://doi.org/10.1016/j.rse.2015.11.027

Phan, L. N. (2012). *Automated rapid thermal imaging systems technology*. MIT - Massachusetts Institute of Technology.

Rakha, T., & Gorodetsky, A. (2018). Review of Unmanned Aerial System (UAS) applications in the built environment: Towards automated building inspection procedures using drones. *Automation in Construction*, *93*(March), 252–264. https://doi.org/10.1016/j.autcon.2018.05.002

Rao, P. K. (1972). Remote sensing of urban heat islands from an environmental satellite. *Bulletin of the American Meteorological Society*, *53*, 647–648.

Rotach, M. W., Voogt, R., Bernhofer, C., Batchvarova, E., Christen, A., Clappier, A., Feddersen, B., Gryning, S.-E., Martucci, G., Mayer, H., Mitev, V., Oke, T. R., Parlow, E., Richner, H., Roth, M., Roulet, Y., Ruffieux, D., Salmond, J. A., Schatzmann, M., Voogt, J. a. (2005). BUBBLE – an Urban Boundary Layer Meteorology Project. *Theoretical and Applied Climatology*, *81*(3–4), 231–261. https://doi.org/10.1007/s00704-004-0117-9

Sobrino, J. A., Oltra-Carrió, R., Jiménez-Muñoz, J. C., Julien, Y., Sòria, G., Franch, B., & Mattar, C. (2012). Emissivity mapping over urban areas using a classification-based approach: Application to the Dual-use European Security IR Experiment (DESIREX). *International Journal of Applied Earth Observation and Geoinformation*, *18*(1), 141–147. https://doi.org/10.1016/j.jag.2012.01.022

Sobrino, J. A., Bianchi, R., Paganini, M., Sòria, G. Jiménez-Muñoz, J. C., Oltra-Carrió, R., Mattar, C., Romaguera, M., Franch, B., Hidalgo, V., Cuenca, J., Julien, Y., Atitar, M., Fernández-Renau, A., Gómez, J.A., Miguel, E., Gutiérrez de la Cámara, Ó., Jiménez, M., Prado, E., Rodríguez-Cantano, R., Ruiz, I., Nerry, F., Najjar, G., Kastendeutch, P., Pujadas, M., Molero, F., Moreno, J., Alonso, L., Fernández, F., Galán, E., Cañada, R., Romero, J. M., Calpe-Maravilla, J., Camps-Valls, G., Bosch-Magraner, M., Puente-Robles, R., Cordero-Salvador, J., Torres-Carrero, J., Duque-Cuesta, M. A., Moya, F., Labajo, A., Labajo, S., Hidalgo-Rodríguez, J., Acero, J. A., Hernández-Martín, E., Martilli, A., Salamanca, F., Gimeno-Presa, L., Pigeon, G.. (2009). *Desirex 2008 - Final Report*.

Sobrino, Jose A., Del Frate, F., Drusch, M., Jiménez-Muñoz, J. C., Manunta, P., & Regan, A. (2016). Review of thermal infrared applications and requirements for future high-resolution sensors. *IEEE Transactions on Geoscience and Remote Sensing*, *54*(5), 2963–2972. https://doi.org/10.1109/TGRS.2015.2509179

Sobrino, José A., & Jiménez-Muñoz, J. C. (2005). Land surface temperature retrieval from thermal infrared data: An assessment in the context of the Surface Processes and Ecosystem Changes Through Response Analysis (SPECTRA) mission. *Journal of Geophysical Research D: Atmospheres*, *110*(16), 1–10. https://doi.org/10.1029/2004JD005588

Tamura, T., Hoyano, A., Hitoshi, A., & Asano, K. (2001). Developing the capturing system of spherical thermograph and applications to built environment. In A. E. Rozlosnik & R. B. Dinwiddie (Eds.), *Proceedings of SPIE Conference on Thermosense* (Vol. 4360, pp. 169–176).

Trigo, I. F., Monteiro, I. T., Olesen, F., & Kabsch, E. (2008). An assessment of remotely sensed land surface temperature. *Journal of Geophysical Research Atmospheres*, *113*(17), 1–12. https://doi.org/10.1029/2008JD010035

Trigo, I. F., Peres, L. F., DaCamara, C. C., & Freitas, S. C. (2008). Thermal land surface emissivity retrieved from SEVIRI/Meteosat. *IEEE Transactions on Geoscience and Remote Sensing*, *46*(2), 307–315. https://doi.org/10.1109/TGRS.2007.905197

Viel, M., Ceriola, G., & Ridder, K. de. (2012). *Urban Heat Island. Final Report: Volume 1* (Vol. 1). Retrieved from http://canterbury.royalcommission.govt.nz/Final-Report-Volume-One-Contents

Voogt, J. A., & Oke, T. . (1998). Effects of urban surface geometry on remotely-sensed surface temperature. *International Journal of Remote Sensing*, *19*(5), 895–921. https://doi.org/10.1080/014311698215784

Voogt, J. a., & Oke, T. R. (1997). Complete Urban Surface Temperatures. *Journal of Applied Meteorology*, *36*(9), 1117–1132.

Voogt, J. A., & Oke, T. R. (2003). Thermal remote sensing of urban climates. *Remote Sensing of Environment*, *86*(3), 370–384. https://doi.org/10.1016/S0034-4257(03)00079-8

Walkie Talkie architect 'didn't realise it was going to be so hot.' (2013). *The Guardian*. Retrieved from https://www.theguardian.com/artanddesign/2013/sep/06/walkie-talkie-architect-predicted-reflection-sun-rays

Watson, K. (1992). Two-temperature method for measuring emissivity. *Remote Sensing of Environment*, *42*(2), 117–121. https://doi.org/10.1016/0034-4257(92)90095-2

Xu, X., Cai, H., Qiao, Z., Wang, L., Jin, C., Ge, Y., Wang, L., Xu, F. (2017). Impacts of park landscape structure on thermal environment using QuickBird and Landsat images. *Chinese Geographical Science*, *27*(5), 818–826. https://doi.org/10.1007/s11769-017-0910-x

Yang, X. (2011). *Urban Remote Sensing: Monitoring, Synthesis and Modeling in the Urban Environment*. https://doi.org/10.1002/9780470979563

Yin, C., Yuan, M., Lu, Y., Huang, Y., & Liu, Y. (2018). Effects of urban form on the urban heat island effect based on spatial regression model. *Science of the Total Environment*, *634*, 696–704. https://doi.org/10.1016/j.scitotenv.2018.03.350

Zhou, D., Xiao, J., Bonafoni, S., Berger, C., Deilami, K., Zhou, Y., Frolking, S., Yao, R., Qiao, Z., Sobrino, J. A. (2019). Satellite Remote Sensing of Surface Urban Heat Islands: Progress, Challenges, and Perspectives. *Remote Sensing*, 1–36. https://doi.org/10.3390/rs11010048

Zhou, D., Zhao, S., Liu, S., Zhang, L., & Zhu, C. (2014). Surface urban heat island in China's 32 major cities: Spatial patterns and drivers. *Remote Sensing of Environment*, *152*, 51–61. https://doi.org/10.1016/j.rse.2014.05.017